Polymethine dyes-loaded solid lipid nanoparticles (SLN) as promising photosensitizers for biomedical applications

Spectrochimica Acta Part A: Molecular and Biomolecular Spectroscopy

Polymethine dyes-loaded Solid Lipid Nanoparticles (SLN) as promising photosensitizers for biomedical applications.

--Manuscript Draft--

Manuscript Number:	
Article Type:	Full Length Article
Section/Category:	Biomolecular and Biomedical Spectroscopy
Keywords:	polymethine dyes; solubility; nanocarrier; SLN; optical imaging; photodynamic activity
Corresponding Author:	Giorgia Chinigò, Ph.D. University of Turin: Universita degli Studi di Torino ITALY
First Author:	Giorgia Chinigò, Ph.D.
Order of Authors:	Giorgia Chinigò, Ph.D.
	Ana Gonzalez-Paredes
	Alessandra Gilardino
	Nadia Barbero
	Claudia Barolo
	Paolo Gasco
	Alessandra Fiorio Pla
	Sonjia Visentin
Abstract:	Polymethine dyes (PMD) have proved to be excellent candidates in the biomedical field for potential applications in both diagnostic and therapeutic. However, PMD application in biomedicine is hindered by their poor solubility and stability in physiological conditions. Therefore, the incorporation of these dyes inside nanosystems could be extremely important to prevent the formation of dye aggregates in aqueous environment and protect the photophysical characteristics. In the present work two PMD based on the benzoindolenine ring (bromine benzo-cyanine-C4 and bromine benzo-squaraine-C4) were incorporated into Solid Lipid Nanoparticles (SLN) to solubilize and stabilize them in aqueous solutions. Obtained SLN showed a high incorporation efficiency for both PMD (≈90%) and not only preserved their spectroscopic properties in physiological conditions but also enhanced their excellent photophysical and photochemical properties in the NIR region. Viability assays showed good biocompatibility of both empty and loaded nanocarriers while the cellular uptake and intracellular localization showed the effective internalization in MCF-7 cells, with a partial mitochondrial localization for CY-SLN. Moreover, in vitro phototoxicity assay showed that cyanine loaded-SLN (CY-SLN) is more photoactive than the free dye.
Suggested Reviewers:	Nora Ventosa ICMAB: Institut de Ciencia de Materials de Barcelona ventosa@icmab.es For her expertise in the field of nanocarriers.
	Anatoliy Tatarets SSI Institute for Single Crystals NAS of Ukraine: Naukovo-tehnologicnij kompleks Institut monokristaliv Nacional'na akademia nauk Ukraini tatarets@isc.kh.ua For his expertise in the synthesis of polymethine dyes for biological applications
	Atanas Kurutos Bulgarian Academy of Sciences: B'lgarska akademia na naukite ohtak@chem.uni-sofia.bg For his expertise in the synthesis of polymethine dyes for biological applications

Dept. of Life Sciences and Systems Biology

University of Torino
V. Accademia Albertina 13
10123, Torino (Italy)

Tel +39 011 6704667
Fax +39 011 6704508

Editor
Spectrochimica Acta Part A: Molecular and Biomolecular Spectroscopy

Date: 20-09-2021
Subject: Submission Original Article

Dear Editor,

We are hereby submitting a manuscript entitled: "**Polymethine dyes-loaded Solid Lipid Nanoparticles (SLN) as promising photosensitizers for biomedical applications**" by Chinigò *et al.* for your consideration for publication in Spectrochimica Acta Part A: Molecular and Biomolecular Spectroscopy.

Cancer is still one of the greatest challenges facing our world and the biological significance of this work perfectly matches these challenges, i.e. the urgent need for more effective diagnostics tools and therapies. Polymethine dyes (PMD) have proved to be excellent candidates for potential biomedical applications in both diagnostic and therapeutic fields. First of all, thanks to their excellent spectroscopic properties exhibited in the near-infrared region, these dyes proved promising diagnostic agents in the field of *in vivo* optical imaging. In addition, recent studies have revealed that some PMD are potential photosensitizers for the photodynamic treatment of some types of tumor. However, due to their highly hydrophobic structure, PMD's application in biomedicine is hindered by their poor solubility and stability in physiological conditions. Hence the need to develop new approaches that allow PMD to be solubilized or screened for their hydrophobicity, thus overcoming the challenges of bioavailability.

Here we investigated the possibility to use Solid Lipid Nanoparticles (SLN) as nanocarriers to improve PMD's solubility and bioavailability in physiological conditions. In particular, we entrapped into SLN a **bromo-functionalized benzoindolenine ring-based cyanine** recently published by our group as a potential photosensitizer for PDT and its **newly synthesized squaraine** derivative which shows enhanced fluorescence performances but which is completely insoluble in aqueous solutions. To the best knowledge of the authors, this paper is the **first example in literature of squaraine's incorporation into SLN**. In summary, we demonstrated that **SLN are a valuable delivery strategy**

for PMD in biomedical applications. In fact, SLN not only allows to solubilize otherwise insoluble and unusable PMD in physiological conditions like our squaraine derivative but even **enhance their spectroscopic performances**. Overall our work demonstrated that PMD incorporation into SLN may increase the value of these dyes as candidates for future *in vivo* imaging and / or PDT applications.

Taking into account the topics covered by Spectrochimica Acta Part A: Molecular and Biomolecular Spectroscopy and in particular the novel applications in photochemistry and photobiology, we believe that our work will be of interest to the readers of the Journal, especially those interested in the potential biomedical applications of dyes. Based on the novelty and impact of our findings, we hope that you will consider our manuscript for publication in Spectrochimica Acta Part A: Molecular and Biomolecular Spectroscopy.

Here are reported the most significant papers published by our groups about PMD's spectroscopic properties and/or PDT applicability:

Ciubini B., Visentin S., Serpe L., Canaparo R., Fin A., and Barbero N., "Design and synthesis of symmetrical pentamethine cyanine dyes as NIR photosensitizers for PDT," *Dye. Pigment*., **160**, 806–813 (2019)
doi: 10.1016/j.dyepig.2018.09.009

Serpe L. *et al.*, "Squaraines bearing halogenated moieties as anticancer photosensitizers: Synthesis, characterization and biological evaluation," *Eur. J. Med. Chem*., **113**, 187–197 (2016)
doi: 10.1016/j.ejmech.2016.02.035

Butnarasu C., Barbero N., Barolo C., and Visentin S., "Interaction of squaraine dyes with proteins: Looking for more efficient fluorescent turn-on probes" *Dye. Pigment*., **184**, 108873 (2021)
doi.org/10.1016/j.dyepig.2020.108873

Barbero N., Butnarasu C., Visentin S., and Barolo C., "Squaraine Dyes: Interaction with Bovine Serum Albumin to Investigate Supramolecular Adducts with Aggregation-Induced Emission (AIE) Properties" *Chem. - An Asian J.*, **14**, 896–903 (2019)
doi: 10.1002/asia.201900055

Alberto G. et al., "Solid silica nanoparticles as carriers of fluorescent squaraine dyes in aqueous media: Toward a molecular engineering approach," *Colloids Surfaces A. Physicochem. Eng. Asp*., **568**, 123–130 (2019)
doi: 10.1016/j.colsurfa.2019.01.052

Yours sincerely,

Giorgia Chinigò and co-authors

Graphical Abstract

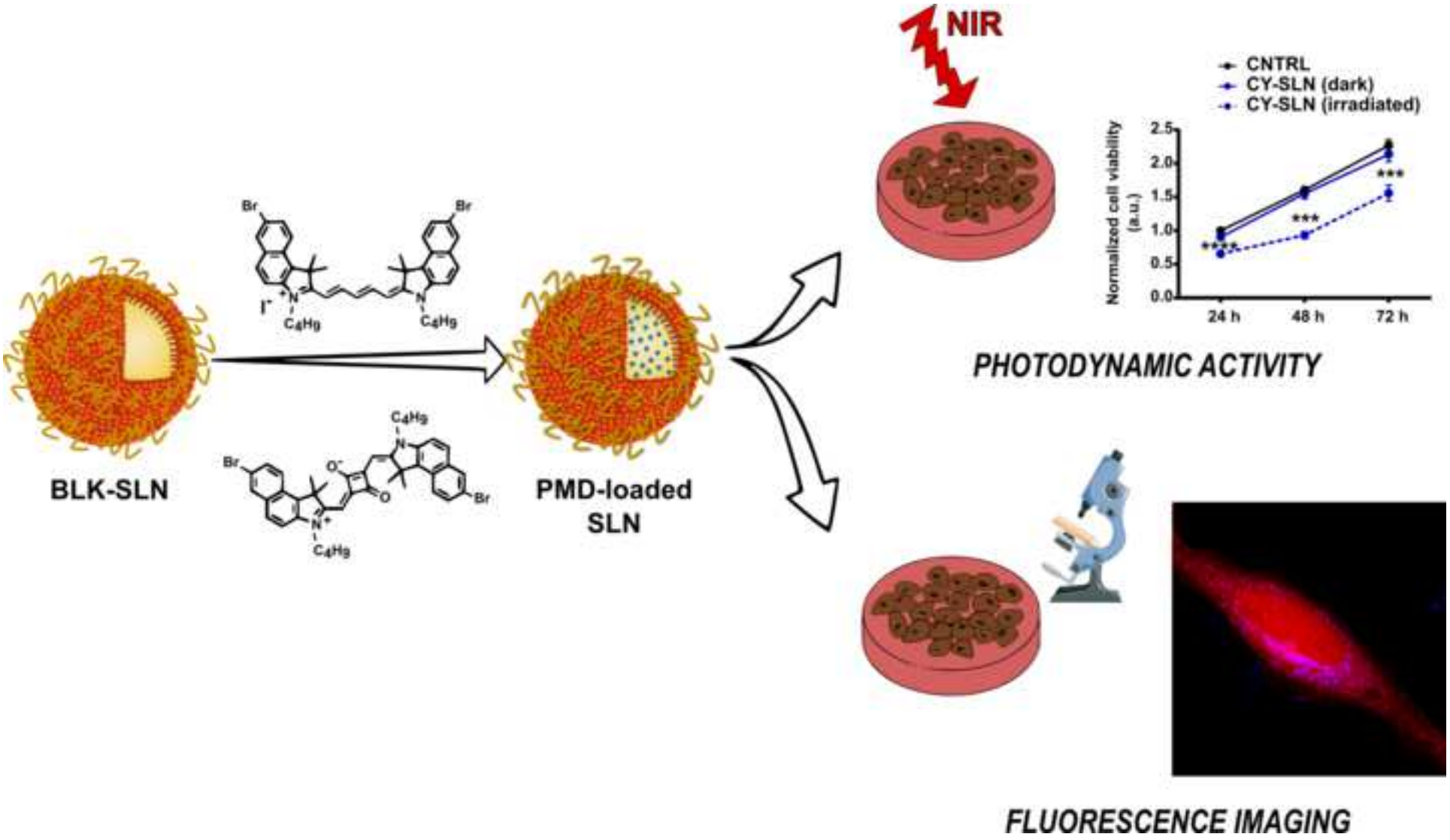

Highlights

- Polymethine dyes are promising diagnostic and therapeutic agents
- Polymethine dyes show poor solubility and stability in physiological conditions
- Solid Lipid Nanoparticles allow dyes' solubilization in physiological conditions
- Dye-loaded nanoparticles show low cytotoxicity and an efficient cellular uptake
- Nanoparticles increase Squaraines' quantum yield and Cyanines' photoactivity

Polymethine dyes-loaded Solid Lipid Nanoparticles (SLN) as promising photosensitizers for biomedical applications.

Giorgia Chinigò[a*]; Ana Gonzalez-Paredes[b,1], Alessandra Gilardino[a], Nadia Barbero[c], Claudia Barolo[c,d], Paolo Gasco[b], Alessandra Fiorio Pla[a†] & Sonja Visentin[e†]

[a] University of Torino, Department of Life Sciences and Systems Biology, Via Accademia Albertina 13, 10123 Turin, Italy

[b] Nanovector Srl, Via Livorno 60, 10144, Turin, Italy

[c] University of Torino, Department of Chemistry, NIS Interdepartmental Centre and INSTM Reference Centre, Via Quarello 15a, 10135, Turin, Italy

[d] ICxT Interdepartmental Centre, Lungo Dora Siena 100, 10153 Turin, Italy

[e] University of Torino, Department of Molecular Biotechnology and Health Science, via Quarello 15a, 10135, Turin, Italy.

* Correspondence: giorgia.chinigo@unito.it

† These authors contributed equally to this paper

**

1 ABSTRACT

Polymethine dyes (PMD) have proved to be excellent candidates in the biomedical field for potential applications in both diagnostic and therapeutic. However, PMD application in biomedicine is hindered by their poor solubility and stability in physiological conditions. Therefore, the incorporation of these dyes inside

[1] Present address: NanoMedMol Group, Instituto de Química Medica (IQM), Consejo Superior de Investigaciones Científicas (CSIC), C/Juan de la Cierva 3, 28006, Madrid, Spain

**Abbreviations

PMD: polymethine dye; NIR: near-infrared; PDT: photodynamic treatment; SLN: solid lipid nanoparticles; CY: cyanine; SQ: squaraine; PS: photosensitizer; DLS: dynamic light scattering; BW: before wash; A3W: after three washes; PDI: polydispersity index; EPR: enhanced permeability and retention; PEG: polyethylene glycol; AF4: asymmetric flow field-flow-fractionation

nanosystems could be extremely important to prevent the formation of dye aggregates in aqueous environment and protect the photophysical characteristics. In the present work two PMD based on the benzoindolenine ring (bromine benzo-cyanine-C4 and bromine benzo-squaraine-C4) were incorporated into Solid Lipid Nanoparticles (SLN) to solubilize and stabilize them in aqueous solutions. Obtained SLN showed a high incorporation efficiency for both PMD (≈90%) and not only preserved their spectroscopic properties in physiological conditions but also enhanced their excellent photophysical and photochemical properties in the NIR region. Viability assays showed good biocompatibility of both empty and loaded nanocarriers while the cellular uptake and intracellular localization showed the effective internalization in MCF-7 cells, with a partial mitochondrial localization for CY-SLN. Moreover, *in vitro* phototoxicity assay showed that cyanine loaded-SLN (CY-SLN) is more photoactive than the free dye.

KEYWORDS: polymethine dyes, solubility, nanocarrier, SLN, optical imaging, photodynamic activity

2 INTRODUCTION

In the last two decades, strong interest has been attracted to bioimaging and therapeutics of near-infrared (NIR) probes. These dyes, thanks to their emission in the NIR region of the electromagnetic spectrum (650-900 nm), which is characterized by minimal scattering of the excitation light and low self-fluorescence of biological molecules, allow deeper tissue penetration with minimal background interference [1]. Among NIR fluorescent probes, NIR polymethine dyes (PMD), such as pentamethine and heptamethine cyanines (CY) and squaraines (SQ), have been extensively studied for many biomedical applications [2], including *in vivo* optical imaging [3], thanks to their peculiar spectroscopic properties, the easiness in designing, the simplicity of synthesis and the close relationship between structure and properties [5,6]. Some NIR PMD have been shown to enhance *in vivo* characterization of tumors, by significantly improving tumor visualization and allowing detection and identification of small pre-neoplastic lesions and metastasis [4,7]. Moreover, it has recently been shown that a unique group of NIR fluorescent heptamethine cyanine preferentially accumulate in cancer cells without the

need for chemical conjugation in many different types of cancer cells including cultured, circulating and disseminated tumor cells [8, 9, 10], as well as in preclinical models, including mice and dogs [8–12]. More interestingly, many studies have recently highlighted an intrinsic anticancer activity of some PMD, which may be used as efficient agents for photothermal and photodynamic therapy (PDT) [2, 13], alternative strategies for the treatment of both oncological and non-oncological diseases [13]. Indeed both cyanine [16–18] and squaraine [19–24] derivatives have shown excellent light-induced toxicity on different types of tumors. Moreover, from data reported in literature, it seems that the presence of a heavy atom in the heterocyclic ring of these dyes leads to greater photodynamic activity, due to the enhancement of the inter-system conversion process, which underlies the singlet oxygen production [18,24,25].

However, the main challenges in the biomedical application of NIR PMD are associated with their structural characteristics, which result in poor solubility and low chemical stability, especially in aqueous solutions. In order to overcome this limit, a valid alternative to the synthetic approach is represented by their incorporation into different nanoparticle systems, which may solubilize or shield hydrophobicity of this class of compounds and, therefore, overcome bioavailability challenges [2,26,27]. Indeed, PMD can be successfully loaded into organic nanoparticles, such as micelles [28,29], liposomes [28] and lipid nanoparticles [31–33]. Among these organic nanosystems, in the last decades, solid lipid nanoparticles (SLN) have proved themselves excellent candidates for the targeting and delivery of various diagnostic [34,35] and therapeutic [34] agents, including photosensitizers (PS) [37,38]. Besides the biocompatibility of the excipients used for their formulation and the possibility of being synthesized through relatively simple and inexpensive processes, they also possess great kinetic stability [34]. Very few examples of incorporation of PMD within SLN are currently reported in literature, regarding indocyanine green (ICG) and some cyanine derivatives based on the indolenine ring (DiO, DiI, DiD, DiR and IR-780) [33,35,39].

Here, we investigated the possibility of using SLN to increase solubility and stability of some NIR PMD in aqueous solutions in view of possible future applications in the biomedical field. In particular, we entrapped into SLN two symmetrical polymethine dyes (CY and SQ) based on an identical heterocyclic moiety, i.e. a bromo-functionalized benzoindolenine ring. The two dyes differ in the polymethine bridge resulting in a positively

charged dye (CY) and a zwitterionic one (SQ) which, in turn, provoque quite different solubility properties in an aqueous solution at physiological pH. In particular, SQ dye, designed following the successful series of Br-indolenine squaraines showing excellent PDT activity [22], suffers from a very low solubility in aqueous media, preventing its use for biological applications. In the present paper, we showed that SLN not only allow to solubilize PMD in aqueous solution, as aimed, but even enhance their spectroscopic performances, making PMD-SLN potential and appealing candidates for *in vivo* imaging and/or PDT applications.

3 MATERIALS AND METHODS

3.1 Materials

All the chemicals for SQ and CY synthesis were purchased from Merck and were used without any further purification. Epikuron® 200 (soybean lecithin with a phosphatidylcholine content ≥92% - Cargill) was purchased from AVG (Italy), trilaurin and benzylalcohol from Fluka, 2-phenylethanol and PEG-40 stearate (Myrj 52) from Sigma Aldrich. NaCl was supplied by ACEF (Italy). Only freshly distilled water and ultra-pure water (Milli-Q, Millipore, USA) were used. Ethanol 96%, Tetrahydrofuran and Acetonitrile (HPLC grade) were purchased from Scharlab (Italy).

NovaChem Surfactant 100 (special mix of non-ionic and ionic detergents for Asymmetric Flow Field-Flow Fractionation (AF4) applications) was purchased from Postnova Analytics GmbH (Germany).

3.2 Synthesis

(**CY**) was synthesized as previously reported by some of us [38]. To obtain (**SQ**), compound **2** (0.45 g, 0.95 mmol) and squaric acid (0.05 g, 0.48 mmol) were introduced in a 10-20 mL microwave vial with a toluene/n-butanol mixture (1:1, 14 mL) and heated at 160 °C for 30 min. After solvent evaporation, Flash column chromatography with 100% CH_2Cl_2 allowed to remove all the impurities. Then elution of 100% acetone afforded the squaraine as blue-green crystals (28%).

MS (ESI) $[M-H]^-$: 765.08

^{1}H NMR (200 MHz, DMSO-d_6) δ: 8.07 – 7.93 (m, 4H), 7.73 (d, J = 8.8 Hz, 2H), 7.59 (dd, J = 9.1, 2.0 Hz, 2H), 7.26 (d, J = 8.8 Hz, 2H), 6.15 (s, 2H), 4.10 (s, 4H), 1.97 (s, 14H), 1.89 – 1.69 (m, 5H), 1.46 (dd, J = 15.3, 7.6 Hz, 5H), 0.95 (t, J = 7.2 Hz, 7H).

^{13}C NMR (50MHz, DMSO-d_6) δ: δ 182.02, 171.28, 139.71, 134.54, 132.13, 131.39, 130.48, 128.61, 126.88, 123.93, 117.82, 111.03, 86.58, 50.88, 43.60, 29.24, 26.61, 20.16, 13.70.

All microwave reactions were performed in single-mode Biotage Initiator 2.5. TLC were performed on silica gel 60 F254 plates. ESI-MS spectra were recorded using LCQ Thermo Advantage Max spectrometer, with electrospray interface and ion trap as mass analyzer. The flow injection effluent was delivered into the ion source using N_2 as sheath and auxiliary gas. ^{1}H NMR (200 MHz) and ^{13}C NMR (50 MHz) spectra were recorded on a Bruker Avance 200 NMR.

3.3 Solid Lipid Nanoparticles (SLN) preparation

Blank (BLK-SLN) and dye-loaded SLN (CY-SLN and SQ-SLN) were prepared in collaboration with Nanovector s.r.l. (Turin, Italy). SLN were prepared by oil-in-water (O/W) warm microemulsion method reported elsewhere [41,42], slightly modified. Briefly, the lipid matrix (trilaurin) was heated above its melting point (52°C) together with phosphatidylcholine and short-chain alcohols, then this lipid phase was mixed under magnetic stirring with an aqueous phase at the same temperature containing the surfactant PEG-40 stearate in order to stabilize O/W interface and promote spontaneous microemulsion formation. When clear microemulsion was formed, it was immediately dispersed into water at the same temperature (52°C) (ratio 1:10 v/v) under mechanical stirring (1900 rpm) and left to achieve room temperature (1900 rpm). Dye-loaded SLN were prepared in the same way by adding the PMD (cyanine or squaraine) to the oil phase of the microemulsion. Obtained SLN dispersions were then washed (3X) by tangential flow filtration (TFF) (Vivaflow 50, RC membrane, 100 KDa MWCO, Sartorius Stedim Italy S.r.l.), for purification, all residual solvents were finally reduced at regulatory acceptable

concentrations [41]. Each formulation (BLK-SLN, CY-SLN and SQ-SLN) was prepared in triplicate to verify the reproducibility of the synthesis procedure and increase the reliability of data.

3.4 Physicochemical characterization

3.4.1 Determination of particle size and surface charge

The average dimension of SLN was evaluated by batch mode Dynamic Light Scattering (DLS), while Zeta potential was measured by Laser Doppler Velocimetry (LDV). For size measurement, SLN dispersions were diluted 1:100 in ultrapure water, whereas for zeta potential measurements samples were diluted 1:50 in NaCl 1mM. All measurements were carried out on Zetasizer-Nano ZS (Malvern Instruments, UK), in triplicate, at 25°C.

3.4.2 Asymmetric Flow Field-Flow fractionation (AF4) characterization

To deeper characterize SLN's size distribution, they were analyzed by AF2000 Asymmetric Flow Field-Flow Fractionation (AF4) instrument (Postnova Analytics GmbH, Germany), which was coupled online to an SPD-20A UV–vis spectrophotometer (Postnova), and a Zetasizer Nano ZS (Malvern Instruments). AF4 was performed in a PMMA channel with a spacer of 350 µm width at the inlet, lined with a regenerated cellulose membrane (cut off 10 KDa). Filtered (0.1 µm Durapore membrane) 0.05% NaCl solution in ultrapure water added with 0.05% Novachem Surfactant 100 was used as the carrier. Samples were diluted 1:2 in the carrier and then manually injected into the system (20 µl). Channel tip flow and focus flow was set to 1 mL/min. The flow rate to the detector was kept at 0.5 mL/min, and the cross flow was set to decrease from 1 mL/min to 0.1 mL/min in 20 minutes and then to remain constant at 0.1 mL/min for 20 minutes. The UV detector was set at 280 nm with a sensitivity of 0.001, and the acquisition time for each autocorrelation function in the Zetasizer Nano detector was 3 seconds. The intensity of scattered light (kcount/s) and ζ-average mean diameter (nm) were elaborated using Zetasizer Nano Software. The dimensional range for each analyzed sample was obtained from the integration of the DLS distribution curve.

3.5 Entrapment efficiency and chemical composition

Dyes entrapment efficiency was calculated as the ratio between dye concentration in SLN dispersion before washing (BW) by TFF and after 3 washing cycles (A3W) according to the following equation:

$$EE\ (\%) = \frac{[dye]A3W}{[dye]BW} \times 100$$

Washing steps were performed by addition and removal of a fixed amount of water, equal to the volume of dispersion.

Dye concentration was determined after SLN disruption by dilution in tetrahydrofuran (1:100). Absorbance was measured by spectrophotometric titration in 99% tetrahydrofuran at 692 nm and 672 nm for cyanine and squaraine samples respectively (UV-visible spectrophotometer - HITACHI UH5300). Dyes concentration inside SLN was calculated by comparing the absorbance of the unknown sample with a calibration curve prepared with standards of known concentrations.

Phosphatidylcholine (PC) content was also determined by HPLC-UV analysis using a method previously described [42], to confirm the final composition of SLN (i.e. after washing steps) and their chemical stability overtime.

3.6 Optical properties of dyes and dye-loaded SLN

Absorbance spectra were recorded on HITACHI UH5300 spectrophotometer (quartz cuvettes, 1 cm pathway length) in ethanol with increasing water content (from 0% to 90%) for dyes' spectroscopic characterization and in 100% ultrapure water for dye loaded SLN. Cyanine's molar extinction coefficient (ε) in absolute ethanol was obtained from Ciubini *et al.* [38], whereas squaraine's molar extinction coefficient (ε) in absolute ethanol was determined by spectrophotometric titration. The analysis was performed in duplicate. Results were considered acceptable once the difference between the determined log ε was less or equal to 0.02 in relevancy to their average.

Fluorescence measurements were recorded on a HORIBA FluoroLog2 (Jobin-Yvon) fluorimeter. Diluted solutions with absorbance around or lower than 0.1 units were used to avoid the presence of aggregates. Because of the low Stokes shift (20 nm for CY and 6 nm for SQ), typical of this class of compounds, emission

spectra were obtained by exciting dyes at the wavelength corresponding to the hypsochromic shoulder showed in absorption spectra (λ_{ex}= 620 nm and 640 nm for cyanine and squaraine respectively)._Dyes' fluorescence spectra were recorded in ethanol with increasing water content (from 0% to 90%) and dye-loaded SLN's emission spectra in 100% ultrapure water. Fluorescence lifetimes (τ_f) were measured in DMSO using a nanoLED source (emission at 636 nm, Horiba Jobin-Yvon) and a single photon counting detector (TBX04 Horiba Jobin-Yvon). Fluorescence quantum yields (ϕ) were determined in DMSO using the same instrument with the integrating sphere Quanta-ϕ (Horiba) and De Mello method. Values reported in results correspond to the average of three independent measurements.

3.7 Cell culture and cell viability assay

Human microvascular endothelial cell line (HMEC-1, American Type Culture Collection ATCC) were cultured in EndoGRO™ MV-VEGF complete medium (Merck Millipore), complemented with 0.5% gentamicin antibiotic and 5 mM L-glutamine; human breast adenocarcinoma cell line (MCF-7, ATCC) were cultured in Dulbecco's Modified Eagle's Medium-high glucose (DMEM from Euroclone), complemented with 10% Fetal Bovine Serum (FBS from Euroclone), 0.5% gentamicin antibiotic and 5 mM L-glutamine. All cell cultures were maintained in an incubator at 37 °C and 5% CO_2 atmosphere, using Falcon™ plates as supports.

For cell viability, cells ($0.5 \cdot 10^4$ cells/well) were seeded in 96-well plates (Sarstedt, Germany). After 18 h incubation at 37°C, different dyes concentrations of dye-loaded SLN dispersions (from 10 nM to 1 µM), were added for 24 and 48 h to the culture medium. In order to compare the cytotoxicity of the dye in the free form or after encapsulation, cytotoxicity of cyanine in the free form was tested (diluted from a stock 1mM in DMSO). SQ alone was not tested due to its insolubility in these conditions. For each condition, eight replicates were performed. Cytotoxicity was assessed 24 and 48 h after SLN treatment using CellTiter 96 AQueous Non-Radioactive cell proliferation assay (Promega, USA) following manufacturer instruction. Briefly, MTS was added (10%) to the culture medium and kept in an incubator for 2 h. Cells without SLN and incubated with complete medium or basal medium without serum and grow factor (EndoGRO starve for HMEC samples and DMEM 0% FBS for MCF-7 samples) were used as positive and negative controls, respectively. Absorbance was then recorded at 490 nm (soluble formazan absorbance) using a microplate reader (FilterMax F5, Multi-Mode Microplate

Reader, Molecular Devices). Absorbance values obtained were analyzed with Excel software (Office, Microsoft) to determine the mean absorbance for each condition after subtraction of the average background (absorbance value of cell medium alone treated with MTS was considered as background). Absorbance values obtained are directly proportional to the number of viable cells.

3.8 Photodynamic treatment and phototoxicity assay

To evaluate the photodynamic activity, MCF-7 cells were plated in 96 well plates ($0.5 \cdot 10^4$ cell/well in 200µL of DMEM 10% FBS) and after six hours were treated with CY-SLN, SQ-SLN and CY at different concentrations (from 10 to 200 nM). Cells were incubated O/N at 37°C and 5% CO_2 and then were irradiated with a light beam intensity of 8 mW/cm^2 for 15 minutes. For cell irradiation, a compact LED array-based illumination system with a homogeneous illumination area was used. The system was specifically designed and produced by Cicci Research s.r.l (Italy) for *in vitro* PDT tests on cells grown in standard multiwell plates (96-wells). The proposed illumination system includes a RED-LED array (light source with excitation wavelength: 640 nm, and irradiance: 8 mW/cm^2) composed of 96 LEDs in a 12 × 8 arrangement. In addition, both LED-array and 96-multiwell plates were placed into a case to isolate the system during irradiation. 24 h, 48 h and 72 h after LED treatment MTS assay were performed in order to evaluate cell viability. For each time monitored (24 h, 48 h and 72 h) two 96-well plates were prepared: one plate was treated with the light beam and the other one was used as control (not irradiated).

3.9 Cellular uptake and intracellular localization

Cells ($50 \cdot 10^4$ cells/dish) were seeded in 10 cm diameter Petri dishes and after three days culture media were removed and replace with fresh culture media. Cells were incubated for 2 h, 6 h, O/N and 24 h with fresh culture media containing the same concentration (100 nM) of cyanine in the free form (CY) or encapsulated into SLN (CY-SLN) and of squaraine encapsulated into SLN (SQ-SLN). Following incubation at 37°C, the medium was removed, cells were trypsinized and the pellet was washed twice with PBS. Proteins were subsequently extracted using 50 µL of RIPA buffer (Pierce® RIPA Buffer, Thermo scientific) and left 1 h on ice. Then cell lysates were sonicated and left on ice for 1 h. After quantification by the BCA Protein Assay proteins were diluted in ethanol

to a final concentration of 1 µg/µL. Then cell lysates were diluted 1:10 in ethanol to a final volume of 1 mL and fluorescence emission of the sample was recorded on a spectrofluorimeter (FluoroLog2, Jobin-Yvon - HORIBA).

To assess the intracellular localization of dye-loaded SLN we used Calcein and MitoTracker Red (Molecular probes®, Invitrogen), in order to label and track the whole cellular volume and mitochondria in live cells, respectively. Briefly, $10 \cdot 10^4$ cells were left to attach for 24 h on glass coverslips in a 6-well plate (Sarstedt, Germany) and then incubated O/N with growth medium containing 100 nM of the dye incorporated into SLN (CY-SLN or SQ-SLN) or of the dye in the free form (CY). After incubation, cells were washed and then incubated with Calcein (250 nM) or MitoTracker Red (250 nM) for 30 min. After incubation, wells were washed twice with Hanks' Balanced Salt Solution (HBSS) in order to wash off the excess probe and fixed in 4% paraformaldehyde (PAF) at 37°C for 2 min. Coverslips were then mounted onto a glass slide by DABCO MIX (purchased from Sigma-Aldrich) and observed using a Leica TCS SP8 confocal system (Leica Microsystems, Germany) equipped with a HCX PL APO 63X/1.4 NA oil-immersion objective. Cyanine and squaraine dyes were excited with a HeNe laser at 633 nm, whereas Calcein and MitoTracker Red were excited with DPSS laser at 561 nm in order to simultaneously detect the probes. Images were acquired on the three coordinates of the space (XYZ planes) with a resolution of 0.081 µm x 0.081 µm x 0.299 µm and were processed and analyzed with ImageJ software (Rasband, W.S., U.S. National Institutes of Health, Bethesda, MA). 3D images with Calcein allowed assessing whether dyes are within the cell or not and Mitotracker Red signals allowed to understand whether dyes co-localize with cell mitochondria (Pearson's correlation coefficient was measured by using ImageJ JACoP plugin).

3.10 Statistical analysis

Data shown are the average values of three independent pulled experiments ± SEM (standard error mean). Statistical analyses were performed using Graph-Pad Prism 6.0 software (La Jolla, CA, USA). Statistical significance between populations was determined by analysis of variance (1way ANOVA-Kruskal Wallis test) followed by *post-hoc* Dunn's multiple comparisons test. Differences with p-values <0.05 were considered statistically significant and *: p-value < 0.05, ***: p-value < 0.0005, ****: p-value < 0001.

4 RESULTS AND DISCUSSION

4.1 Synthesis of polymethine dyes

The synthesis of symmetrical brominated pentamethine cyanine and squaraine dyes involved the condensation of the quaternary heterocyclic salts (**2**), bearing an activated methyl group, with a malonodialdehyde derivative and squaric acid, respectively. Compound **1** was obtained from 7-bromo-1,1,2-trimethyl-1Hbenzo[e]indole exploiting the Fischer indole synthesis by reacting (6-bromonaphthalen-2-yl) hydrazine with 3-methylbutan-2-one in glacial acetic acid, as previously described [38]. The quaternization of the benzoindolenine ring to get compound **2**, performed under microwave irradiation, led to an increased acidity of the methyl group which enabled the following condensation reaction (Fig. 1 A) to obtain CY and SQ. The synthesis of the symmetrical cyanine dye is already reported in our previous work [38], while the symmetrical squaraine dye was synthesized in a one-step reaction under microwave heating following our well-established method for indolenine-based squaraines [43] by reacting two equivalents of quaternary heterocyclic salts with squaric acid (Fig. 1 A).

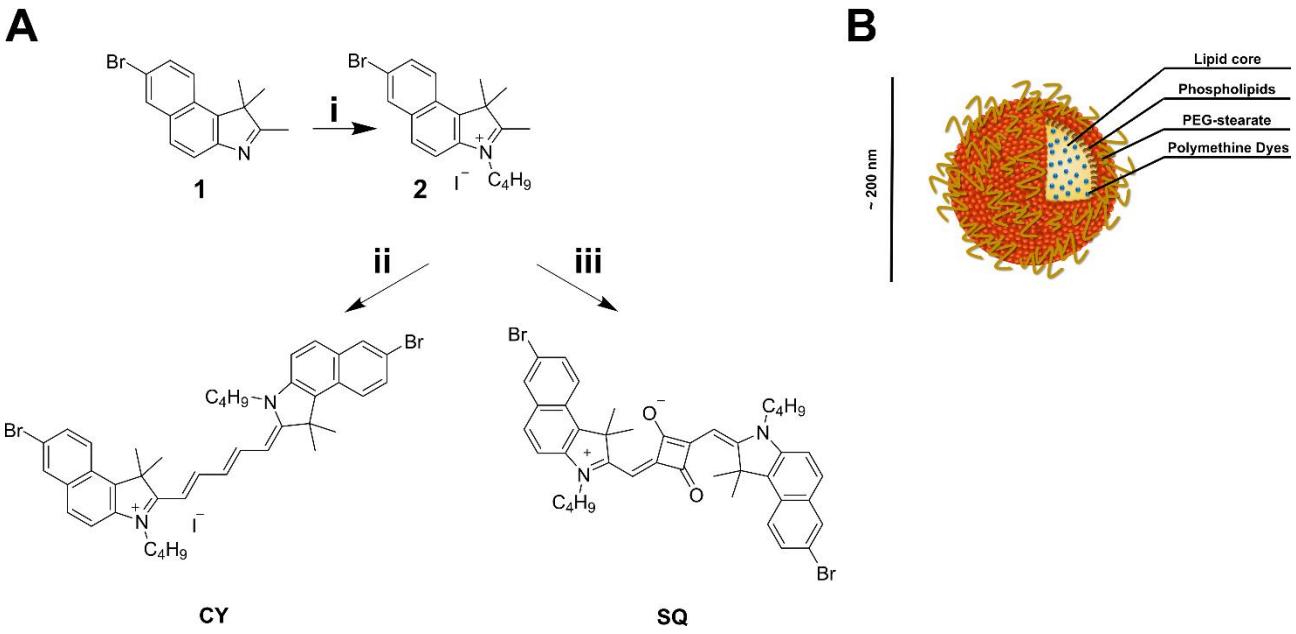

Figure 1. PMD and SLN.

A) PMD synthesis: (i) acetonitrile, iodobutane, MW, 45 min, 155 °C; (ii) sodium acetate, acetic anhydride, N-((1E,2E)-3-(phenylamino)allylidene)benzenaminium chloride, MW, 10 min, 130 °C; (iii) squaric acid, toluene/n-butanol, MW, 30 min, 160 °C. **B**) Schematic representation of dye-loaded SLN synthesized.

4.2 Solid Lipid Nanoparticles (SLN) preparation and physicochemical characterization

Solid Lipid Nanoparticles (SLN) and dye-loaded SLN were prepared as reported in the experimental section. Results of SLN physicochemical characterization through batch mode dynamic light scattering (DLS) for each formulation after the purification procedure (A3W) are reported in Table 1. BLK-SLN exhibited a mean diameter of 171 nm and a polydispersity index (PDI) lower than 0.20, which indicates the homogeneity of size distribution. On the other hand, the characterization of dye-loaded SLN (CY-SLN and SQ-SLN) revealed higher sizes due to the presence of the PMD within the nanoparticles and slightly higher PDI that remained anyway lower than 0.30. A schematic representation of the dye-loaded SLN synthesized is represented in Figure 1 B. It is important to highlight that synthesized particles have a mean diameter around 200 nm, which is highly interesting in cancer applications. Indeed, previous studies on liposomes of different mean size [44] set at 200 nm the threshold size for more effective extravasation of nanoparticles into the tumor tissues via the leaky vessels by the enhanced permeability and retention (EPR) effect [45]. Moreover, the presence of the steric stabilizer PEG-40 stearate into the formulation will probably improve the bioavailability of the nanosystem in body fluids and its pharmacokinetic profile after administration for further potential *in vivo* studies [46]. Indeed, PEG chains sterically stabilize nanoparticles and increase their plasma half-life, reducing binding to serum proteins and other opsonic factors [47]. Moreover, both blank and dye-loaded SLN showed good stability under storage at different temperatures (4, 25 and 40 °C): as shown in Figure S1 A, size and PDI of all SLN did not change over 30 days from their synthesis at all three investigated temperatures.

Regarding the ζ-potential, BLK-SLN showed a value of -11.6 mV, comparable to other SLN prepared with triglycerides [48], suggesting good stability of the dispersion. Comparing ζ-potentials measured on the loaded

294 SLN (Table 1), we observed a significant difference between the two formulations: SQ-SLN showed a negative ζ-
295 potential as well as BLK-SLN, whereas CY-SLN showed an inversion of ζ-potential, which becomes positive.
296 Considering the structures of the two PMD (Fig. 1 B) and the positive charge associated with the cyanine dye,
297 the inversion of the potential observed in the case of CY-SLN can be due to a partial localization of the dye on
298 the particle surface. This effect has been also described for other cyanine dyes incorporated in lipid nanocarriers
299 [49].

300

301 ***Table 1***

302 *Physicochemical properties of BLK-SLN, SQ-SLN and CY-SLN. PDI: polydispersity index; ZP: zeta potential, EE: entrapment*
303 *efficiency; PC: phosphatidylcholine (mean ± SD, n = 3).*

SLN	Size (nm)	PDI	ZP (mV)	EE (%)	PC (mg/mL)
BLK-SLN	170.9 ± 22.84	0.152 ± 0.052	-11.6 ± 4.9	-	11.05 ± 1.50
CY-SLN	194.7 ± 27.43	0.258 ± 0.036	+7.8 ± 2.2	89.2 ± 0.4	11.60 ± 1.00
SQ-SLN	203.4 ± 18.43	0.250 ± 0.052	-6.6 ± 2.3	88.9 ± 7.4	9.96 ± 1.78

304

305 Finally, in order to deeper physicochemical characterization and to verify the effective size distribution of
306 the formulation obtained through batch mode DLS, SLN were also analyzed employing Asymmetric Flow Field-
307 Flow-Fractionation (AF4), an elution-based particle separation technique that allows to separate, detect and
308 measure any sub-populations eventually present in the colloidal sample. This technique is based on the
309 application of a force field (cross flow) perpendicular to the particle transport direction, which allows smaller
310 particles to be transported faster and eluted earlier [50]. AF4 analysis confirmed that all 3 types of SLN prepared
311 were characterized by one main population: the fractograms, reported in Figure 2, show an upward trend of
312 hydrodynamic size over the elution peaks. The diameters calculated by analysis of light scattered signals
313 corresponding to peak elution were respectively 143 nm for BLK-SLN (Fig. 2 A), 182 nm for CY-SLN (Fig. 2 B) and
314 157nm for SQ-SLN (Fig. 2 C). The elution volume (mL), corresponding to the elution time (min), and peak width
315 are displayed in Table 2.

316 The difference with respect to the diameter obtained from the batch mode DLS measurement may be due
317 to the different ionic composition of the buffer used in AF4, compared to ultrapure water used for the batch

mode. Indeed, the different ionic and surfactant composition of the medium alters the nature of the ionic sphere that surrounds the surface of nanoparticles and, consequently, their hydrodynamic radius, which includes not only the diameter of the nanoparticle itself but also the ions included within the slipping plane, which move together to it in Brownian motion. Moreover, a small shoulder was detected before the elution peak of CY-SLN (6.5 mL <elution volume <10.6 mL). Nevertheless, because of the low intensity of the peak close to the noise threshold, this signal is not attributable to the presence of a sub-population of SLN within the sample, but it probably indicates the formation of small micellar systems (64 nm) induced by the surfactants present in the elution medium used (Novachem 0.05% + NaCl 0.05%) and probably related to the different surface characteristics showed by positive ζ-potential of CY-SLN compared with the other formulations [51].

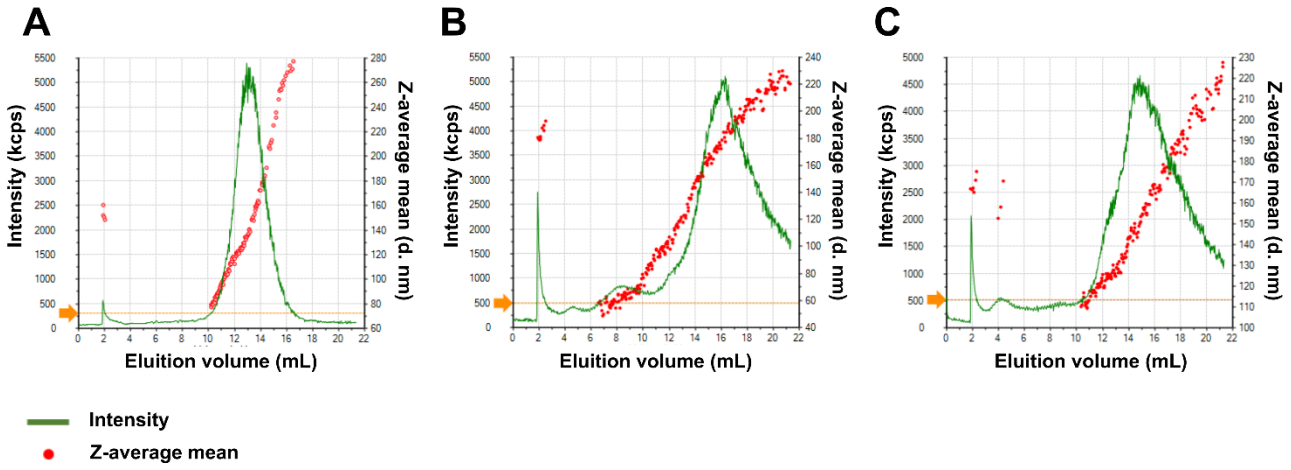

Figure 2. SLN AF4 characterization.

AF4-DLS fractograms of BLK-SLN (A), CY-SLN (B) and SQ-SLN (C) (red dots: z-average mean diameter in nm; green curve: intensity of scattered light in kcount/s; yellow line: noise threshold).

Table 2

Particle size obtained from DLS analysis of AF4 fractograms, elution volume (mL) and peak width.

SLN type	Z-average mean diameter (nm)	Elution volume (mL) (initial-final)	Peak width (nm)
BLK-SLN	143	10.5-16	32.0
CY-SLN	182	12.5-21	27.2
SQ-SLN	157	11-20	25.2

The entrapment efficiency of SLN was very high for both dyes, with values close to 90% (Table 1), showing the efficacy of this type of lipid carrier for the incorporation of hydrophobic molecules. Moreover, the PC concentrations displayed in Table 1 confirmed the final composition of SLN and negligible losses during the purification process, as PC content after 3 washes was about 90% compared to that of non-washed formulations.

4.3 Dyes and dye-loaded SLN optical characterization

CY and SQ dyes show a narrow absorption band in the Far-Red, perfectly matching the phototherapeutic window (Fig. 3 A). CY (Fig. 3 A-I) and SQ (Fig. 3 A-II) show similar optical properties in absolute ethanol with an absorbance maximum at 688 (CY) and 668 (SQ) nm, preceded by a hypsochromic shoulder typical for PMD [24] (at about 620 and 640 nm respectively) and emission maxima at 708 (CY) and 674 nm (SQ). CY and SQ exhibit high molar extinction coefficients ($2.08 \cdot 10^5$ and $2.52 \cdot 10^5$ $L \cdot mol^{-1}$ cm^{-1}, respectively, in ethanol) and good quantum yields in organic solvent (36% and 31% respectively in DMSO). The higher molar extinction coefficient showed by SQ as compared to CY is due to the greater rigidity of squaraine derivatives' polymethinic bridge, which reduces photoisomerization phenomena leading to a more stable structure and an optimization of its optical properties with respect to the corresponding cyanine derivative. The squaraine derivative's absorption/emission spectrum shows a typical hypsocromic shift compared with the corresponding cyanine derivative, because of the presence in its structure of the squaric acid core that balances the positive charge present on the heterocyclic nitrogen.

However, both dyes are poorly soluble in aqueous solutions and this compromises their applicability in the biomedical field, as well as that of other organic dyes. Indeed, as shown in Figures 3 B and 3 C, absorption spectra of CY (Fig. 3 B-I) and SQ (Fig. 3 C-I) in ethanol show a significant change in shape and intensity upon increasing the water content from 0 to 90%, leading to the bleaching of their fluorescent properties (Fig. 3 B-II for CY and Fig. 3 C-II for SQ). The modifications of the absorption spectra upon water addition suggest the rapid

aggregate formation of the two dyes in aqueous conditions. This phenomenon is particularly evident in the case of SQ dye, which exhibits a lower solubility than CY in aqueous solution due to its zwitterionic structure.

Interestingly, the incorporation of the PMD into SLN allows to preserve their standard spectroscopic properties even in aqueous solution (Fig. 3 D and 3 E). Indeed, dye-loaded SLN reproduce the same spectroscopic profile exhibited by dyes in the free form in organic solvent with a small bathochromic shift (Table 3). The absorption below 600 nm, shown by dye-loaded SLN, may be due to the Rayleigh scattering from nanoparticles and it is more pronounced in the case of SQ-SLN because of the lower dyes/lipids (w/w) ratio as compared to CY-SLN's one. SQ-SLN quantum yield in H_2O is even higher than the one exhibited by free-dye in DMSO (52% versus 31%) (Table 3). We also evaluated and compared the fluorescence lifetime (τ_f) of the free-dyes and the dye-loaded SLN. Free-dyes' fluorescence lifetimes (τ_f) show mono-exponential decay and are in the nanoseconds range, accordingly with the previous results [38]. As regard dye-loaded SLN, the mono-exponential trend of the τ_f indicates a homogeneous dispersion of the dyes within the lipidic nanosystem in both formulations. Moreover, τ_f recorded for dye-loaded SLN in aqueous solution are similar to those obtained for free-dyes in organic solvent. Interestingly, squaraine into SLN shows again enhanced optical performances with respect to its free form with a fluorescence lifetime even doubled (2.571 versus 1.382). This means that the SQ derivative into SLN gives rise to prolonged fluorescence emission, probably due to an increased stabilization of the fluorophore by the lipidic microenvironment. Finally, we also investigated the stability of the optical properties of the dyes into SLN. Both CY-SLN and SQ-SLN showed good stability until 30 days after formulation (at 4°C and 25°C) and only a small decrease in fluorescence intensity was observed keeping the sample at 40°C (condition of accelerated stability) for 30 days (Fig. S1 B).

These results clearly show that the incorporation of PMD into SLN allows a successful preservation of their optical characteristics, making them suitable candidates for optical imaging.

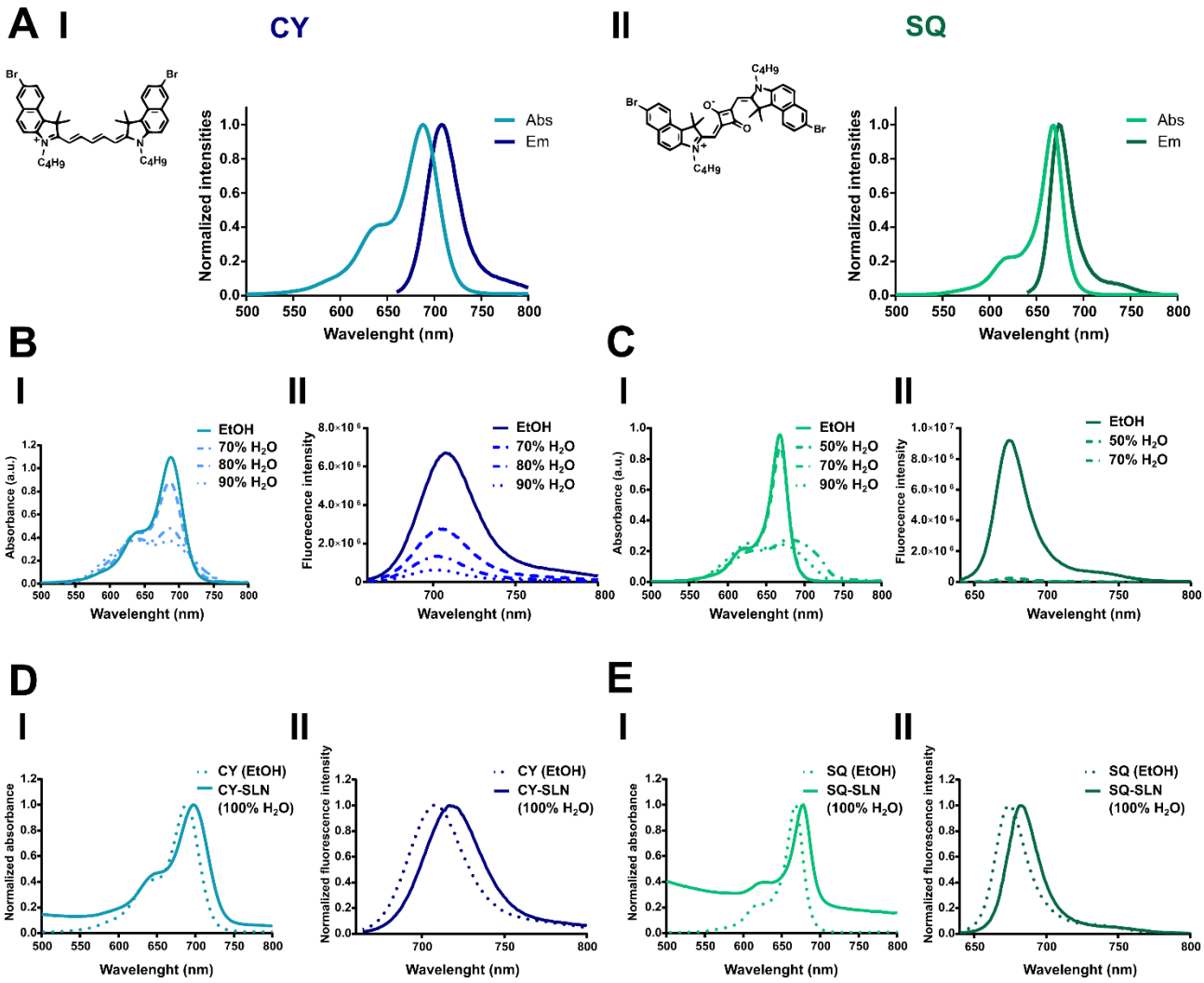

Figure 3. Dyes and dye-loaded SLN optical characterization.

A) Normalized absorption (abs) and emission (em) spectra of CY (I) and SQ (II) in absolute ethanol. Insets show dyes' structures. **B**) Changes in the absorption spectra (I) and in the emission spectra (II) of CY ($5*10^{-6}$ and $5*10^{-7}$ M respectively in absolute ethanol) upon increasing content of water from 0 to 90%. λ_{ex} for emission spectra = 620 nm. **C**) Changes in the absorption spectra (I) and in the emission spectra (II) of SQ ($3*10^{-6}$ and $3*10^{-7}$ M respectively in absolute ethanol) upon increasing content of water from 0 to 90%. λ_{ex} for emission spectra = 640 nm. **D**) Normalized absorption (I) and emission (II) spectra of CY encapsulated into SLN (CY-SLN) in 100% water. Dot lines represent normalized absorption (I) and emission (II) spectra of CY in the free form in absolute ethanol. **E**) Normalized absorption (I) and emission (II) spectra of SQ encapsulated into SLN (SQ-SLN) in 100% water. Dot lines represent normalized absorption (I) and emission (II) spectra of SQ in the free form in absolute ethanol.

Table 3

Optical properties of free-dyes (CY and SQ) in organic solvent and dye-loaded SLN (CY-SLN and SQ-SLN) in aqueous solution. λ_{max}(abs), λ_{max}(em): dyes absorption and emission maxima, respectively, ε: molar extinction coefficient at the absorption maximum, φ_{fl}: fluorescence quantum yield, τ_f: fluorescence lifetime.

	absorbance		emission				
	λ_{max} (nm)	ε λ_{max} (L mol^{-1}cm^{-1})	λ_{max} (nm)	ϕ_{fl} (%)		τ_f (ns)	
	EtOH/H_2O	EtOH	EtOH/ H_2O	DMSO	H_2O	DMSO	H_2O
CY	688	$2.08 \cdot 10^5$	708	36	-	1.570 ± 0.004	-
CY-SLN	698	-	717	-	36	-	1.372 ± 0.004
SQ	668	$2.52 \cdot 10^5$	674	31	-	1.382 ± 0.003	-
SQ-SLN	678	-	682	-	52	-	2.571 ± 0.004

4.4 *In vitro* cell viability of CY-SLN and SQ-SLN

We investigated the inherent cytotoxicity of BLK-SLN, CY-SLN and SQ-SLN using the MTS viability assay on MCF-7 cells. BLK-SLN showed good biocompatibility (Fig. 4 A-I), starting to affect cell viability 24 h after treatment only at the highest lipid concentration tested (about 100 µg/mL, corresponding to a dye concentration of 1.5 µM and 1 µM for CY and SQ respectively). Regarding dye-loaded SLN, cell viability was tested by varying dyes' concentration into SLN in the nanomolar range, in order to identify the maximum concentration at which treatment can be administered without inducing cytotoxicity. CY cytotoxicity in its free form was also tested and Figure 4 A shows that CY (Fig. 4 A-II) started to affect cell viability from a concentration of 400 nM 24 h after treatment, whereas surprisingly, once incorporated into SLN its cytotoxicity increased starting from a concentration of 200 nM 24 h after treatment although with partial recovery at 48h (Fig. 4 A-III). On the contrary, SQ-SLN (Fig. 4 A-IV) are less cytotoxic and do not affect cell viability until a dye concentration of 1 µM. To check the cell-type specificity of the observed CY-SLN cytotoxic effect, we measured CY-SLN cytotoxicity also on endothelial cells (HMECs) and, surprisingly, CY-SLN do not show the same cytotoxic profile shown on MCF-7 (Fig. S2). Indeed, HMECs treated with 200 nM of CY-SLN still show a slight increase in cell viability as compared to the control even 48 h after treatment (Fig. S2). Similar results were also found testing BLK-SLN cytotoxicity on HMECs at lipid concentrations corresponding to those used for CY-SLN treatment (Fig. S2). On the other hand, CY cytotoxicity in the free form did not show any differences between the two cell types, at least in the

concentration range investigated (till 200 nM) (Fig. S2). These results indicate that SLN's and CY-SLN's cytotoxicity is cell type-dependent and it may also suggest that tumor cells may be more sensitive to the dye-loaded nanosystem than normal cells. For subsequent characterizations of our nanosystems on tumor cell model (MCF-7) we used SLN with dye concentrations of 100 nM, in order to avoid results affected by any cytotoxic effects (Fig. 5 A-I).

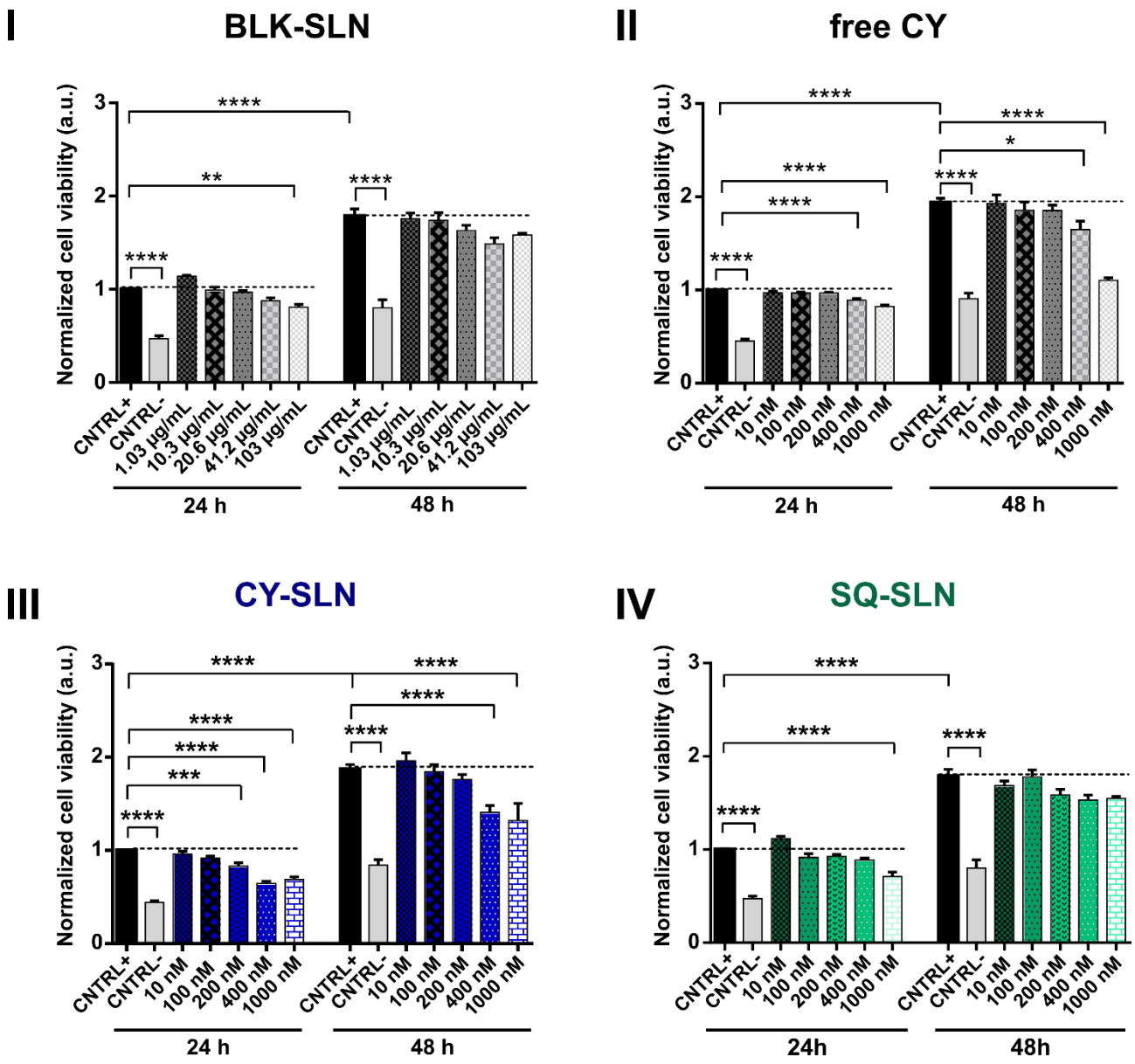

Figure 4. *In vitro* cytotoxicity of CY-SLN and SQ-SLN on MCF-7.

Cell viability assays on MCF-7 24 h and 48 h after treatment with different concentrations of BLK-SLN (**I**), free CY (**II**), CY-SLN (**III**) and SQ-SLN (**IV**). For BLK-SLN concentrations refer to phosphatidylcholine content ([PC] from 1.03 to 103 µg/mL), whereas for dye-loaded SLN concentrations refer to dyes incorporated into SLN (from 10 to 1000 nM). Data are normalized on CNTRL+ (MCF-7 untreated) at 24 h and are represented as mean ± SEM. Data refer to a pull of at least 3 independent

experiments (eight replicates for each experiment). Statistical significance versus CNTRL+: *** P< 0.001, **** P< 0.0001 (Kruskal-Wallis test with *post-hoc* Dunn's test).

4.5 *In vitro* photoactivity of CY-SLN and SQ-SLN

In vitro phototoxicity results, illustrated in Figure 5 A-II, do not show any phototoxic effects of CY in the free form (100 nM) on MCF-7, but interestingly, highlight a photoactivity of CY after encapsulation into SLN (100 nM) (Fig. 5 A-II, CY-SLN versus CNTRL 24 h and 48 h after light beam treatment: p-value < 0.0001 and after 72 h: p-value < 0.001). This result may be due to the lower possibility of aggregation of CY encapsulated into SLN, which leads to an increase in the lifetime of the triplet state leading to a more efficient photoactivity. Alternatively, the photoactivity of CY-SLN could be due to a higher local concentration of the dye due to the nanoencapsulation. Notably, BLK-SLN did not show any phototoxicity, meaning that the decrease in cell viability after light beam treatment is exclusively due to the activity of the dye (Fig. 5 A-II). Our results are in agreement with other studies about potential PS loaded into SLN, that have shown how the incorporation of these highly hydrophobic molecules in lipid nanoparticles may increase their photostability and also their singlet oxygen production capacity [37, 38]. On the other hand, it has to be noticed that the same CY previously tested in its free form resulted in a significant phototoxic activity at 10 nM on HT-1080 [38]. Surely the higher energy fluency rates applied in the previous work (18.0 J/cm^2 versus 7.2 J/cm^2) can at least partially explain the difference in the observed results. However, this difference is probably also attributable to a cell line-dependent sensibility to PMD treatment that emerged even in the dark: indeed, HT-1080 cells showed significant cytotoxicity starting from 100 nM [38], whereas MCF-7 viability was not affected by free CY till 400 nM (Fig. 5 A-II). Regarding the squaraine derivative, it was not possible to investigate its phototoxicity in the free form because of its insolubility in aqueous solutions. However, SQ-SLN do not show any phototoxic effects at the concentration investigated (100 nM) (Fig. 5 B-I), suggesting that this nanosystem could be used as potential diagnostic tools for *in vivo* fluorescence imaging, but not as a therapeutic tool in photodynamic treatment. On the contrary, preliminary data on CY-SLN suggest that they may be tested in photodynamic treatment of some types of cancer, thanks to

its negligible cytotoxicity in the dark and its moderate activity after light beam treatment, enhanced by its incorporation in lipid nanocarriers (Fig. 5 A-I and II).

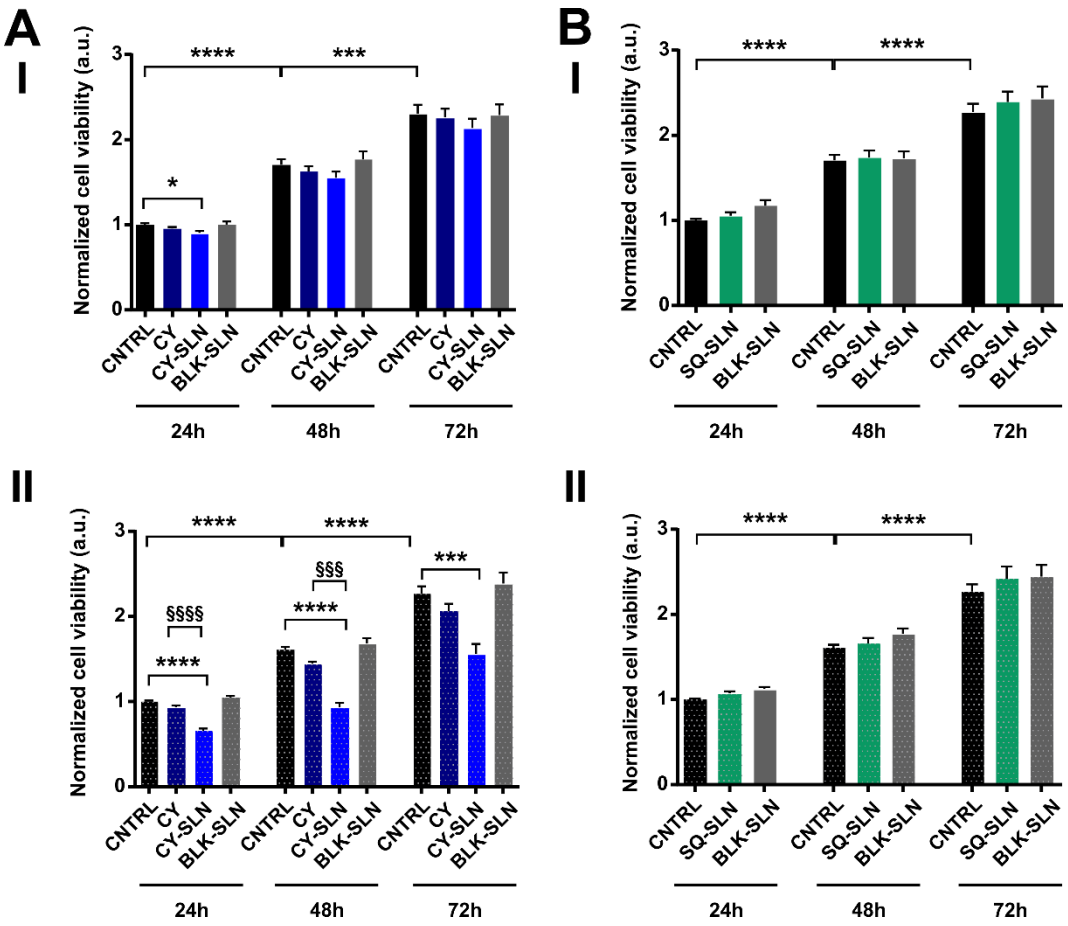

Figure 5. Dyes and dye-loaded SLN *in vitro* phototoxicity

A) Cell viability assays on MCF-7 O/N treated with 100 nM CY (in free form or encapsulated into SLN) kept in the dark (I) or 24 h, 48 h and 72 h after LED irradiation (640 nm, 7.2 J/cm^2) (II). **B**) Cell viability assays on MCF-7 O/N treated with 100 nM SQ (encapsulated into SLN) kept in the dark (I) and 24 h, 48 h and 72 h after LED irradiation (640 nm, 7.2 J/cm^2) (II). Data are normalized on CNTRL at 24 h and represented as mean ± SEM. Data refer to 4 independent experiments (eight replicates for each experiment). Statistical significance versus CNTRL (MCF-7 untreated with dyes): * P< 0.05, *** P< 0.001, **** P< 0.0001; statistical significance between free dyes and dye-loaded SLN: §§§ P< 0.001, §§§§ P< 0.0001 (Kruskal-Wallis test with *post-hoc* Dunn's test).

4.6 Cell uptake and intracellular localization

As mentioned in the introduction, the development of good diagnostic and therapeutic agents in biomedicine requires a setup of positive interactions between the molecule and the cellular system. Indeed, the

474 nanosystem must be internalized efficiently and with reasonable timing by the target cell to reach a good drug
475 delivery performance. Therefore, we investigated the cellular uptake and the intracellular localization of SLN.
476 The cell uptake timings of the synthesized fluorescent nanosystems were analyzed by measuring the
477 fluorescence intensity relative to cell lysates after incubation of MCF-7 cells with CY-SLN and SQ-SLN (dyes
478 concentration: 100 nM) for four different incubation times (2 h, 6 h, O / N and 24 h). An efficient time-dependent
479 accumulation of the dyes was observed in cells treated with dye-loaded SLN, with an appreciable uptake starting
480 from 2 hours in both samples (Fig. 6 A-I: CY-SLN, λ_{em} = 708 nm; Fig. 6 A-II: SQ-SLN, λ_{em} = 674 nm). CY-SLN uptake
481 reaches a plateau after O/N incubation (Fig. 6 A-I). The tailing of the peak observed after 24 h incubation is most
482 likely due to the presence of phenol red (λ_{em} = 674 nm at pH 7) in the culture medium. In order to compare the
483 cell uptake of CY in the free form and CY encapsulated into SLN, we perform the same assay on MCF-7 cells
484 treated with 100 nM of CY in culture media for four different incubation times (Fig. S3). At 100 nM, it seems that
485 the presence of the nanocarrier slows down the internalization of the dye. Indeed, comparing Figure 6 A-I and
486 Figure S3 A it results evident that the fluorescence intensities related to the free dye are strongly more intense
487 than those relating to the incorporated dye. However, it is difficult to establish a replicable ratio between the
488 two signals because it changes with sample and biological variability (n=3).

489 In order to verify the effective internalization of the nanosystem into the cell, excluding the possibility that
490 fluorescence signals recorded from cell lysates came from particles attached on the cell surface, we performed
491 confocal laser scan microscopy experiments on MCF-7 cells treated O/N with 100 nM of dyes incorporated into
492 SLN. The whole cellular volume was labeled using Calcein (red signals in Fig. 6 B and S3 B) and images were
493 acquired on the three coordinates of the space (XYZ), allowing to reconstruct the 3D cellular volume and
494 therefore to check whether dyes fluorescent signals were included within the cellular volume or not. Figure 6 B
495 clearly shows that both types of loaded-SLN are internalized by MCF-7 after O/N incubation. Indeed, in cells
496 treated with CY-SLN (Fig. 6 B-I) or SQ-SLN (Fig. 6 B-II) several fluorescent spots were detected (λ_{ex} = 633 nm)
497 within the cell volume labeled with Calcein. Results obtained from samples treated with cyanine in the free form
498 show, instead, a greater amount of intracellular labeling and a more widespread and delocalized signal of the
499 dye on the entire cell volume as compared to CY-SLN (Fig. S3 B), suggesting higher internalization of the free CY.

500 This result may be explained on one hand by the cationic nature of CY, which may promote its interaction with
501 the cell surface and on the other hand by the overexpression of organic anion-transporting polypeptide (OATP)
502 channels in tumor cells, which may increase its internalisation [3]. On the contrary, the incorporation of the
503 cyanine derivative into the lipid nanoparticle not only may limit its interaction with the plasma membrane,
504 partially masking the positive charge associated with the dye, but also alters its molecular internalization
505 mechanism, which, in fact, in this case, is mediated by an endocytotic mechanism [52]. Finally, comparing CY (Fig.
506 S3 B) and CY-SLN (Fig. 6 B-I) signals it is also possible to detect the greater compartmentalization of cyanine signal
507 when incorporated within the nanoparticle system: compared to the non-specific and diffuse signal given by the
508 dye in its free form, incorporation into a solid lipid matrix allows to obtain a more localized signal.
509 It has been suggested that mitochondria are a major subcellular site for photosensitizer localization and
510 that both cyanine and squaraine dyes localize in mitochondria organelles [4,24]. We, therefore, decided to
511 further investigate the subcellular localization of CY-SLN, staining MCF-7 mitochondria with MitoTracker Red (red
512 signals in Fig. 6 C and S3 C) and to evaluate its co-localization with the dye. Figure 6 C shows that CY-SLN is mainly
513 located in close proximity to mitochondrial regions. A partial co-localization with mitochondria was observed
514 also for CY in the free form as shown in Figure S3 C, although a more widespread signal of the dye on the entire
515 cell volume was observed. These data suggest that the cyanine derivative, both in its free form and encapsulated
516 into SLN, partially associates with the mitochondria once it has penetrated into the cells and this could be linked
517 to its photodynamic activity (Fig. 5 A-II and [38]).

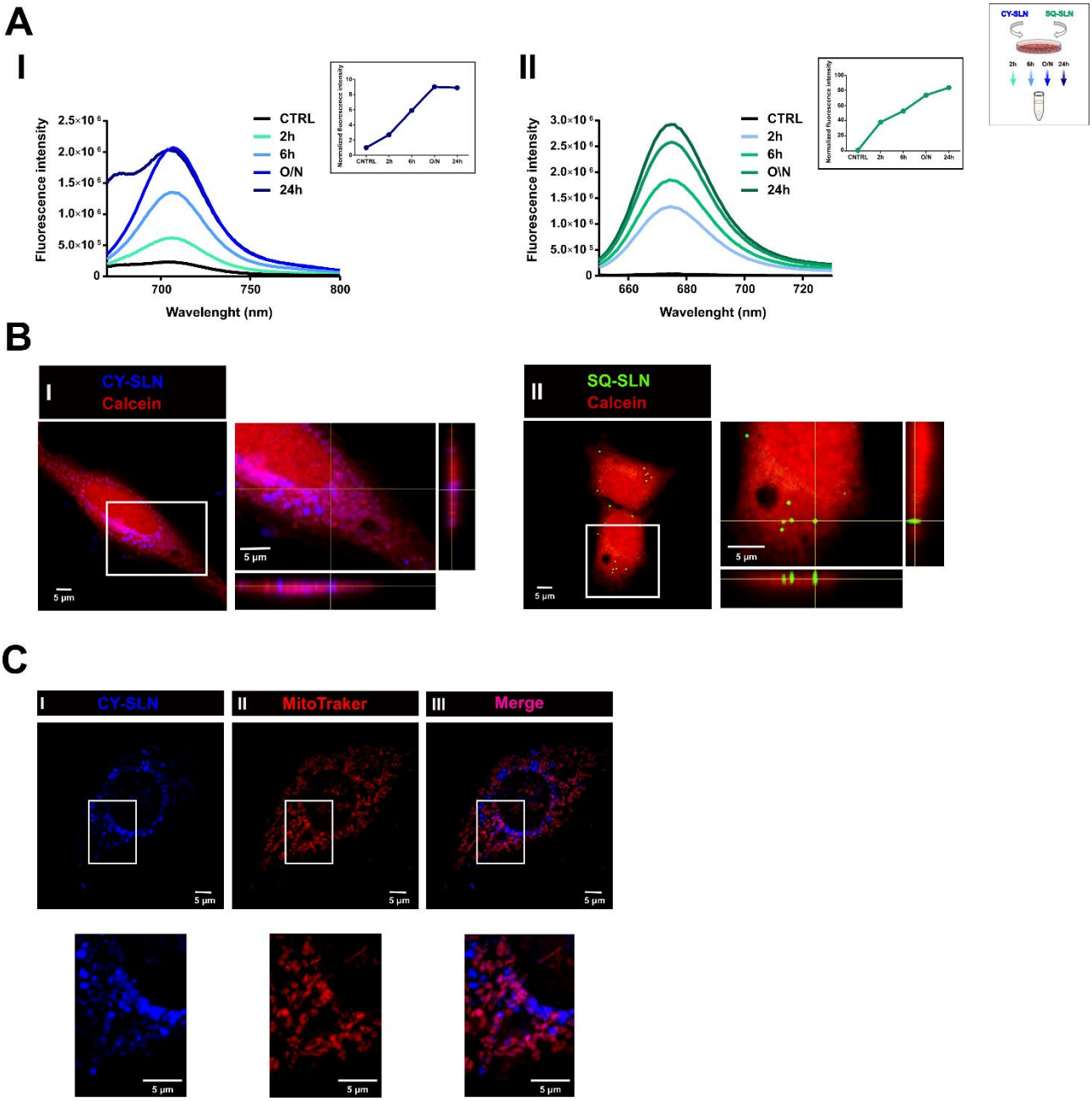

Figure 6. Dye-loaded SLN uptake and intracellular localization.

A) Fluorescence intensity relative to MCF-7 cellular lysates after incubation with 100 nM CY-SLN (I) or SQ-SLN (II) for increasing time intervals (2 h, 6 h, O/N and 24 h). Emission spectra were recorded excitating CY-SLN and SQ-SLN at 620 and 640 nm, respectively. Insets show the trend over time of fluorescence intensity normalized on the control (untreated cells). Data refer to one representative experiment of at least three. On the right a scheme representing cell uptake assay.

B) Representative confocal fluorescence images of MCF-7 cells incubated O/N with either CY-SLN (I) or SQ-SLN (II) at the same concentration (100 nM). Red signal refers to calcein (excitation at 561 nm) and blue/green signal refers to CY-SLN and SQ-SLN respectively (excitation at 633 nm). For each image zoom on a region of interest (indicated by white box) with orthogonal views are reported. Scale bar: 5 µm.

C) Representative confocal fluorescence images of MCF-7 cells incubated O/N with CY-SLN (100 nM). Blue signal in panel I refers to CY-SLN (excitation at 633 nm) and red signal in panel II refers to MitoTracker Red (excitation at 561); panel III:

merged image of panel I and II (pink for overlapped regions); below: zoom on a region of interest indicated by white box. Scale bar: 5 µm.

5 CONCLUSIONS

We successfully incorporated two polymethine dyes (a cyanine CY and a squaraine SQ) based on bromo benzoindolenine ring into SLN in order to overcome their solubility issues in aqueous solutions. Dye-loaded SLN displayed a homogeneous size of <200 nm and high entrapment efficiency, preserving dyes' excellent spectroscopic properties. This study is the first example in the literature of incorporation of a squaraine derivative into SLN, which not only permits the solubilization of this dye (completely insoluble in water), but even enhances its spectroscopic performances with higher ϕ_{fl}. This data, together with the low cytotoxicity of the system and its efficient cellular uptake, suggest that SQ-SLN may be a suitable and appealing candidate as diagnostic agent in *in vivo* optical imaging. On the other hand, CY-SLN, beyond the good optical properties shown, led to a photoactivity on MCF-7 cells. Moreover, CY-SLN seem to have a good uptake and a partial mitochondrial localization, suggesting their potential application as PS for photodynamic anticancer treatment.

In summary, SLN are a valuable delivery strategy for PMD in biomedical applications, although further investigation on *in vivo* models is needed in order to assess the real applicability of these nanosystems in both diagnostic and therapeutic fields.

6 AUTHOR CONTRIBUTIONS

SV, AFP and GC conceived the study; GC synthetized nanoparticles and performed chemical characterization and cell culture experiments; GC wrote the paper and designed the figures; AG performed immunofluorescence and confocal acquisitions; NB synthetized PMD; AGP supervised SLN's synthesis and characterization, performed A4F experiments and wrote A4F results; SV, AFP, CB and PG supervised experiments. All authors revised the manuscript.

7 FUNDING

This work was supported by the University of Torino (Ricerca Locale ex-60%, Linea A, Bando 2020), by the Fondazione CRT (II tornata 2019 RF.2019.2260) and by Compagnia di San Paolo (Bando ex-post – Anno 2018).

8 ACKNOWLEDGEMENTS

We thank Dr. Marta Gai and the Open Lab of Advanced Microscopy at the Molecular Biotechnology Center (OLMA@MBC) for support.

9 REFERENCES

[1] X. M. Yi, F. L. Wang, W. J. Qin, X. J. Yang, and J. L. Yuan, "Near-infrared fluorescent probes in cancer imaging and therapy: An emerging field," *Int. J. Nanomedicine*, vol. 9, no. 1, pp. 1347–1365, 2014, doi: 10.2147/IJN.S60206.

[2] C. Butnarasu, N. Barbero, C. Barolo, and S. Visentin, "Squaraine dyes as fluorescent turn-on sensors for the detection of porcine gastric mucin: A spectroscopic and kinetic study," *J. Photochem. Photobiol. B Biol.*, vol. 205, no. January, p. 111838, 2020, doi: 10.1016/j.jphotobiol.2020.111838.

[3] C. Shi, J. B. Wu, and D. Pan, "Review on near-infrared heptamethine cyanine dyes as theranostic agents for tumor imaging, targeting, and photodynamic therapy," *J. Biomed. Opt.*, vol. 21, no. 5, p. 50901, 2016, doi: 10.1117/1.JBO.21.5.050901.

[4] N. Barbero, S. Visentin, and G. Viscardi, "The different kinetic behavior of two potential photosensitizers for PDT," *J. Photochem. Photobiol. A Chem.*, vol. 299, pp. 38–43, 2015, doi: 10.1016/j.jphotochem.2014.11.002.

[5] N. Barbero, C. Butnarasu, S. Visentin, and C. Barolo, "Squaraine Dyes: Interaction with Bovine Serum

Albumin to Investigate Supramolecular Adducts with Aggregation-Induced Emission (AIE) Properties," *Chem. - An Asian J.*, vol. 14, no. 6, pp. 896–903, 2019, doi: 10.1002/asia.201900055.

[6] W. K. Moon *et al.*, "Enhanced Tumor Detection Using a Folate Receptor-Targeted Near-Infrared Fluorochrome Conjugate," *Bioconjug. Chem.*, vol. 14, no. 3, pp. 539–545, May 2003, doi: 10.1021/bc0340114.

[7] X. Yi *et al.*, "IR-780 dye for near-infrared fluorescence imaging in prostate cancer," *Med. Sci. Monit.*, vol. 21, pp. 511–517, 2015.

[8] C. Shao, C. P. Liao, P. Hu, C. Y. Chu, L. Zhang, and M. H. Bui, "Detection of live circulating tumor cells by a class of near-infrared heptamethine carbocyanine dyes in patients with localized and metastatic prostate cancer," *PLoS One*, vol. 9, no. 2, p. e88967 1-11, 2014.

[9] X. Yang *et al.*, "Optical Imaging of Kidney Cancer with Novel Near Infrared Heptamethine Carbocyanine Fluorescent Dyes," *J. Urol.*, vol. 189, no. 2, pp. 702–710, Feb. 2013, doi: 10.1016/j.juro.2012.09.056.

[10] J. B. et al. Wu, "Near-infrared fluorescence imaging of cancer mediated by tumor hypoxia and HIF1alpha/OATPs signaling axis," *Biomaterials*, vol. 35, no. 28, pp. 8175–8185, 2014.

[11] C. et al. Shi *et al.*, "Heptamethine carbocyanine dye-mediated near-infrared imaging of canine and human cancers through the HIF-1alpha/OATPs signaling axis," *Oncotarget*, vol. 5, no. 20, pp. 10114–10126, Oct. 2014, doi: 10.18632/oncotarget.2464.

[12] R. Krejcir *et al.*, "Anticancer pentamethinium salt is a potent photosensitizer inducing mitochondrial disintegration and apoptosis upon red light illumination," *J. Photochem. Photobiol. B Biol.*, vol. 209, no. March, p. 111939, 2020, doi: 10.1016/j.jphotobiol.2020.111939.

[13] A. M. Rkein and D. M. Ozog, "Photodynamic therapy," *Dermatol. Clin.*, vol. 32, no. 3, pp. 415–425, 2014, doi: 10.1016/j.det.2014.03.009.

[14] S. et al. Luo, "A multifunctional heptamethine near-infrared dye for cancer theranosis," *Biomaterials*, vol. 34, no. 9, pp. 2244–2251, 2013.

[15] X. et al. X. Tan, S. Luo, D. Wang, Y. Su, T. Cheng, and C. Shi, “A NIR heptamethine dye with intrinsic cancer targeting, imaging and photosensitizing properties,” *Biomaterials*, vol. 33, no. 7, pp. 2230–2239, 2012, doi: 10.1016/j.biomaterials.2011.11.081.

[16] J. et al. Atchison *et al.*, “Iodinated cyanine dyes: a new class of sensitisers for use in NIR activated photodynamic therapy (PDT),” *Chem. Commun.*, vol. 53, no. 12, pp. 2009–2012, 2017, doi: 10.1039/C6CC09624G.

[17] D. Ramaiah, I. Eckert, K. T. Arun, L. Weidenfeller, and B. Epe, “Squaraine dyes for photodynamic therapy: study of their cytotoxicity and genotoxicity in bacteria and mammalian cells.,” *Photochem. Photobiol.*, vol. 76, no. 6, pp. 672–677, 2002, doi: 10.1562/0031-8655(2002)076<0672:SDFPTS>2.0.CO;2.

[18] D. Ramaiah, I. Eckert, K. T. Arun, L. Weidenfeller, and B. Epe, “Squaraine Dyes for Photodynamic Therapy: Mechanism of Cytotoxicity and DNA Damage Induced by Halogenated Squaraine Dyes Plus Light (>600 nm)¶,” *Photochem. Photobiol.*, vol. 79, no. 1, p. 99, 2004, doi: 10.1562/0031-8655(2004)79<99:sdfptm>2.0.co;2.

[19] V. Rapozzi, L. Beverina, P. Salice, G. A. Pagani, M. Camerin, and L. E. Xodo, “Photooxidation and Phototoxicity of π-Extended Squaraines,” *J. Med. Chem.*, vol. 53, no. 5, pp. 2188–2196, Mar. 2010, doi: 10.1021/jm901727j.

[20] R. R. Avirah, D. T. Jayaram, N. Adarsh, and D. Ramaiah, “Squaraine dyes in PDT: from basic design to in vivo demonstration,” *Org. Biomol. Chem.*, vol. 10, no. 5, pp. 911–920, 2012, doi: 10.1039/C1OB06588B.

[21] M. S. Soumya, K. M. Shafeekh, S. Das, and A. Abraham, “Symmetrical diiodinated squaraine as an efficient photosensitizer for PDT applications: Evidence from photodynamic and toxicological aspects,” *Chem. Biol. Interact.*, vol. 222, pp. 44–49, 2014, doi: 10.1016/j.cbi.2014.08.006.

[22] L. Serpe *et al.*, “Squaraines bearing halogenated moieties as anticancer photosensitizers: Synthesis, characterization and biological evaluation,” *Eur. J. Med. Chem.*, vol. 113, pp. 187–197, 2016, doi: 10.1016/j.ejmech.2016.02.035.

[23] D. Ramaiah, A. Joy, N. Chandrasekhar, N. V. Eldho, S. Das, and M. V. George, “Halogenated Squaraine Dyes as Potential Photochemotherapeutic Agents. Synthesis and Study of Photophysical Properties and Quantum Efficiencies of Singlet Oxygen Generation,” *Photochem. Photobiol.*, vol. 65, no. 5, pp. 783–790, 1997, doi: 10.1111/j.1751-1097.1997.tb01925.x.

[24] G. Alberto *et al.*, “Solid silica nanoparticles as carriers of fluorescent squaraine dyes in aqueous media: Toward a molecular engineering approach,” *Colloids Surfaces A Physicochem. Eng. Asp.*, vol. 568, no. January, pp. 123–130, 2019, doi: 10.1016/j.colsurfa.2019.01.052.

[25] I. Miletto *et al.*, “Mesoporous silica nanoparticles incorporating squaraine-based photosensitizers: A combined experimental and computational approach,” *Dalt. Trans.*, vol. 47, no. 9, pp. 3038–3046, 2018, doi: 10.1039/c7dt03735j.

[26] A. Kirchherr, A. Briel, and K. Ma, “Stabilization of Indocyanine Green by Encapsulation within Micellar Systems,” *Mol. Pharm.*, vol. 6, no. 2, pp. 480–91, 2009.

[27] S. Sreejith *et al.*, “Near-Infrared Squaraine Dye Encapsulated Micelles for in Vivo Fluorescence and Photoacoustic Bimodal Imaging,” *ACS Nano*, vol. 9, no. 6, pp. 5695–5704, 2015, doi: 10.1021/acsnano.5b02172.

[28] D. Zhang *et al.*, “Nano-confined squaraine dye assemblies: New photoacoustic and near-infrared fluorescence dual-modular imaging probes in vivo,” *Bioconjug. Chem.*, vol. 25, no. 11, pp. 2021–2029, 2014, doi: 10.1021/bc5003983.

[29] I. Texier *et al.*, “Cyanine-loaded lipid nanoparticles for improved in vivo fluorescence imaging,” *J. Biomed. Opt.*, vol. 14, no. 5, pp. 054005 1–11, 2009, doi: 10.1117/1.3213606.

[30] A. Jacquart *et al.*, “LipImage™ 815: novel dye-loaded lipid nanoparticles for long-term and sensitive in vivo near-infrared fluorescence imaging,” *J. Biomed. Opt.*, vol. 18, no. 10, pp. 101311 1–9, 2013, doi: 10.1117/1.JBO.18.10.101311.

[31] J. Mérian, R. Boisgard, P. A. Bayle, M. Bardet, B. Tavitian, and I. Texier, “Comparative biodistribution in

mice of cyanine dyes loaded in lipid nanoparticles," *Eur. J. Pharm. Biopharm.*, vol. 93, pp. 1–10, 2015, doi: 10.1016/j.ejpb.2015.03.019.

[32] S. Morel, E. Terreno, E. Ugazio, S. Aime, and M. R. Gasco, "NMR relaxometric investigations of solid lipid nanoparticles (SLN) containing gadolinium (III) complexes," *Eur. J. Pharm. Biopharm.*, vol. 45, no. 2, pp. 157–163, 1998.

[33] J. Gravier *et al.*, "Lipidots: competitive organic alternative to quantum dots for in vivo fluorescence imaging," *J. Biomed. Opt.*, vol. 16, no. 9, pp. 096013 1–10, 2011, doi: 10.1117/1.3625405.

[34] N. Yadav, S. Khatak, U. Vir, and S. Sara, "Solid lipid nanoparticles - a review," *Int. J. Appl. Pharm.*, vol. 5, no. 2, pp. 8–18, 2013.

[35] A. M. Lima *et al.*, "Hypericin encapsulated in solid lipid nanoparticles: Phototoxicity and photodynamic efficiency," *J. Photochem. Photobiol. B Biol.*, vol. 125, pp. 146–154, 2013, doi: 10.1016/j.jphotobiol.2013.05.010.

[36] F. P. Navarro *et al.*, "Preparation and characterization of mTHPC-loaded solid lipid nanoparticles for photodynamic therapy," *J. Photochem. Photobiol. B Biol.*, vol. 130, pp. 161–169, 2014, doi: 10.1016/j.jphotobiol.2013.11.007.

[37] J. Merian, R. Boisgard, X. Decleves, B. Theze, I. Texier, and B. Tavitian, "Synthetic Lipid Nanoparticles Targeting Steroid Organs," *J. Nucl. Med.*, vol. 54, no. 11, pp. 1996–2003, Nov. 2013, doi: 10.2967/jnumed.113.121657.

[38] B. Ciubini, S. Visentin, L. Serpe, R. Canaparo, A. Fin, and N. Barbero, "Design and synthesis of symmetrical pentamethine cyanine dyes as NIR photosensitizers for PDT," *Dye. Pigment.*, vol. 160, no. September 2018, pp. 806–813, 2019, doi: 10.1016/j.dyepig.2018.09.009.

[39] M. R. Gasco, L. Priano, G. P. Zara, and H. S. S., "Solid lipid nanoparticles and microemulsions for drug delivery: The CNS," in *Progress in Brain Research, Elsevier*, 2009, pp. 181–192.

[40] E. Ugazio, R. Cavalli, and M. R. Gasco, "Incorporation of cyclosporin A in solid lipid nanoparticles (SLN),"

Int. J. Pharm, vol. 241, pp. 341–344, 2002.

[41] "ICH guideline Q3C (R6) on impurities: guideline for residual solvents.," in *European Medicine Agency*, 2016.

[42] A. González-Paredes *et al.*, "Solid lipid nanoparticles for the delivery of anti-microbial oligonucleotides," *Eur. J. Pharm. Biopharm.*, vol. 134, no. November 2018, pp. 166–177, 2019, doi: 10.1016/j.ejpb.2018.11.017.

[43] N. Barbero *et al.*, "Microwave-Assisted Synthesis of Near-Infrared Fluorescent Indole-Based Squaraines," *Org. Lett.*, vol. 17, no. 13, pp. 3306–3309, 2015, doi: 10.1021/acs.orglett.5b01453.

[44] F. Yuan *et al.*, "Vascular permeability in a human tumor xenograft: molecular size dependence and cutoff size.," *Cancer Res.*, vol. 55, no. 17, pp. 3752–6, Sep. 1995.

[45] D. Peer, J. M. Karp, S. Hong, O. C. Farokhzad, R. Margalit, and R. Langer, "Nanocarriers as an emerging platform for cancer therapy," *Nat. Nanotechnol.*, vol. 2, no. 12, pp. 751–760, 2007, doi: 10.1038/nnano.2007.387.

[46] P. L. Turecek, M. J. Bossard, F. Schoetens, and I. A. Ivens, "PEGylation of Biopharmaceuticals: A Review of Chemistry and Nonclinical Safety Information of Approved Drugs," *J. Pharm. Sci.*, vol. 105, no. 2, pp. 460–475, 2016, doi: 10.1016/j.xphs.2015.11.015.

[47] M. Üner and G. Yener, "Importance of solid lipid nanoparticles (SLN) in various administration routes and future perspective," *Int. J. Nanomedicine*, vol. 2, no. 3, pp. 289–300, 2007.

[48] M. A. Schubert and C. C. Muller-Goymann, "Characterisation of surface-modified solid lipid nanoparticles (SLN): Influence of lecithin and nonionic emulsifier," *Eur J Pharm Biopharm*, vol. 61, no. 1–2, pp. 77–86, 2005, doi: 10.1016/j.ejpb.2005.03.006.

[49] G. Lollo, A. Gonzalez-paredes, M. Garcia-fuentes, P. Calvo, D. Torres, and M. J. Alonso, "Polyarginine Nanocapsules as a Potential Oral Peptide Delivery Carrier," *J. Pharm. Sci.*, vol. 106, no. 2, pp. 611–618, 2017, doi: 10.1016/j.xphs.2016.09.029.

[50] A. Zattoni, B. Roda, F. Borghi, V. Marassi, and P. Reschiglian, “Flow field-flow fractionation for the analysis of nanoparticles used in drug delivery,” *J. Pharm. Biomed. Anal.*, vol. 87, pp. 53–61, 2014, doi: 10.1016/j.jpba.2013.08.018.

[51] F. Caputo *et al.*, “Measuring Particle Size Distribution by Asymmetric Flow Field Flow Fractionation: A Powerful Method for the Preclinical Characterization of Lipid-Based Nanoparticles,” *Mol. Pharm.*, vol. 16, no. 2, pp. 756–767, 2019, doi: 10.1021/acs.molpharmaceut.8b01033.

[52] T. G. T. Iversen, T. Skotland, and K. Sandvig, “Endocytosis and intracellular transport of nanoparticles: Present knowledge and need for future studies,” *Nano Today*, vol. 6, no. 2, pp. 176–185, 2011, doi: 10.1016/j.nantod.2011.02.003.

10 Supplemental Information

Figure S1

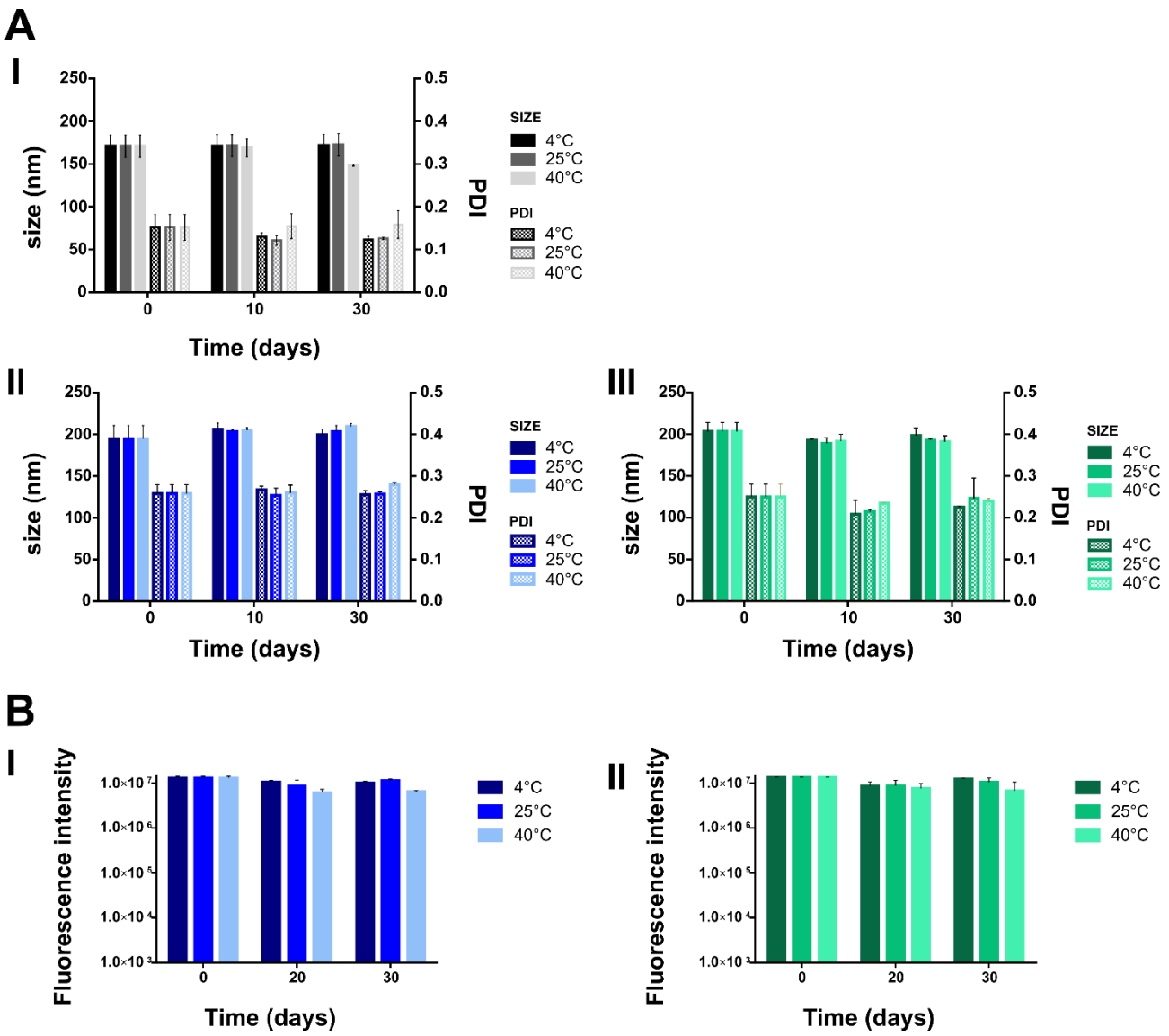

Figure S1. SLN stability

A) Change overtime of size and PDI of BLK-SLN (I), CY-SLN (II) and SQ-SLN (III) at three different storage temperature (4°C, 25°C and 40°C). B) Change overtime of fluorescence intensity of CY-SLN (I) and SQ-SLN (II). Data are expressed as mean ± SEM (n=3).

Figure S2

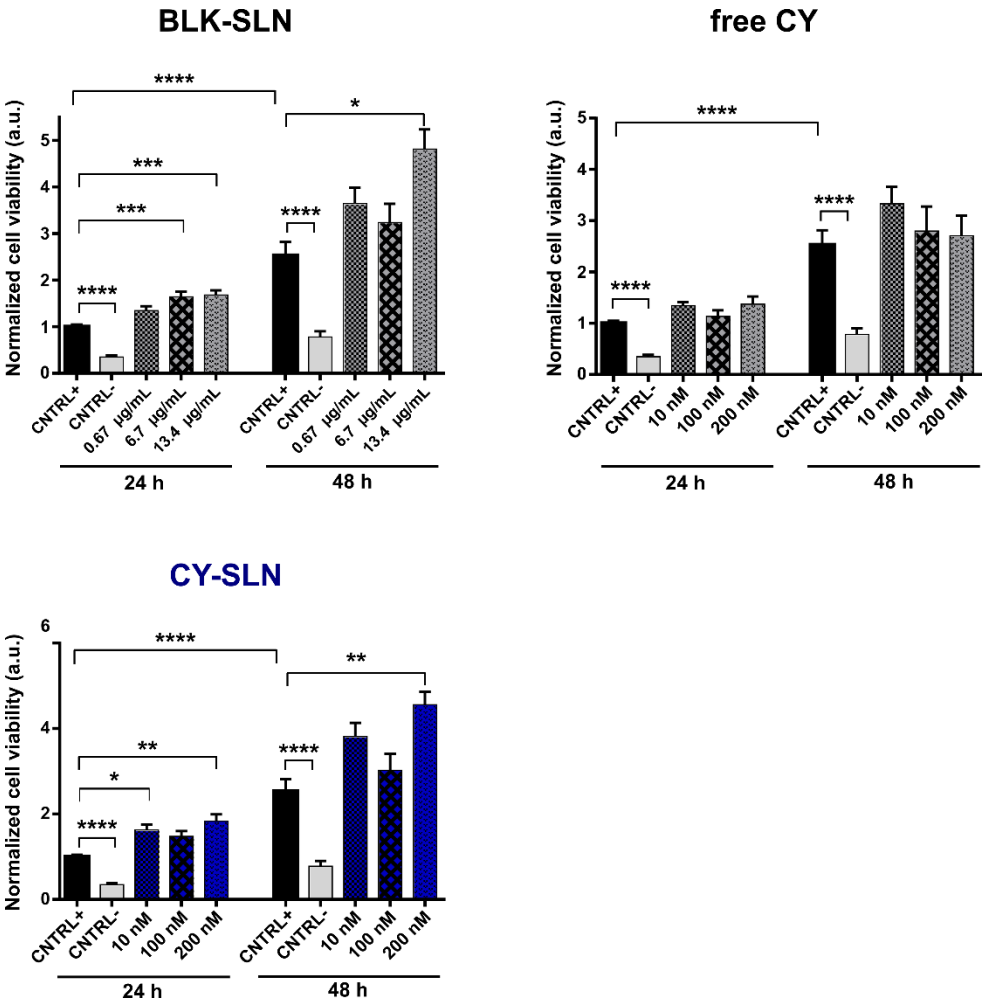

Figure S2. *In vitro* cytotoxicity of CY-SLN and SQ-SLN on HMEC.

Cell viability assays on HMEC 24 h and 48 h after treatment with different concentrations of BLK-SLN, free CY and CY-SLN. For dye-loaded SLN concentrations refer to dyes incorporated into SLN (from 10 to 200 nM) whereas for BLK-SLN concentrations refer to phosphatidylcholine content ([PC] from 0.67 to 13.4 µg/mL corresponding to that of loaded-SLN tested. Data are normalized on CNTRL+ at 24 h and are represented as mean ± SEM. Data refer to at least 3 independent experiments (eight replicates for each experiment). Statistical significance versus CNTRL+ (HMEC untreated with dyes): *** P< 0.001, **** P< 0.0001 (Kruskal-Wallis test with *post-hoc* Dunn's test).

Figure S3

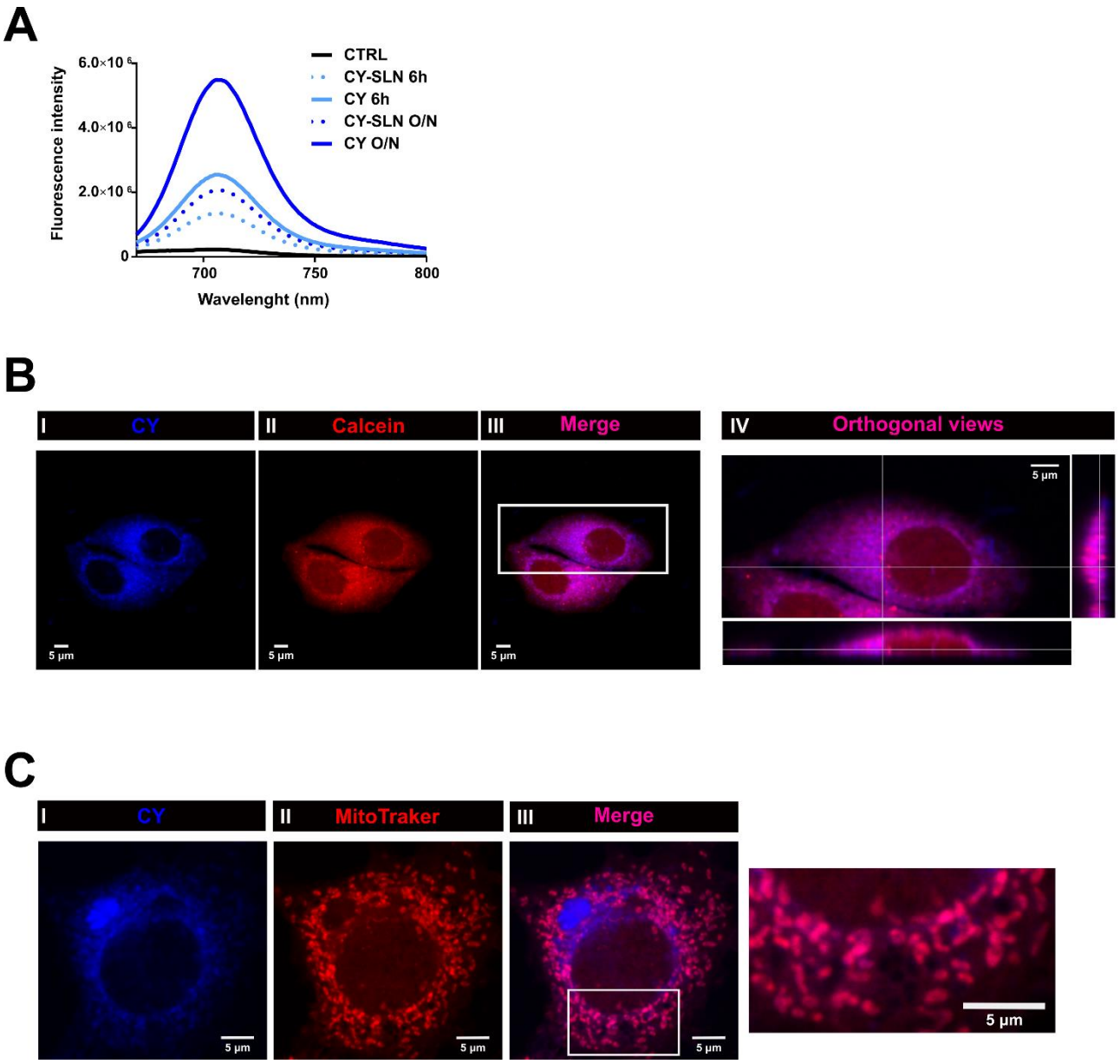

Figure S3. CY uptake and intracellular localization.

A) Fluorescence intensity relative to MCF-7 cellular lysates after incubation with either CY (continuous lines) or CY-SLN (dot lines) at the same concentration (100 nM) for two different time intervals (6 h and O/N). Data refer to one representative experiment of three.

B) Representative confocal fluorescence images of MCF-7 cells incubated O/N with CY (100 nM). Blue signal in panel I refers to dye-loaded SLN (excitation at 633 nm) and red signal in panel II refers to Calcein (excitation at 561 nm); panel III: merged image of panel I and II (pink for overlapped regions); panel IV: zoom on panel III with orthogonal views. Scale bar: 5 µm.

C) Representative confocal fluorescence images of MCF-7 cells incubated O/N with CY (100 nM). Blue signal in panel I refers to CY (excitation at 633 nm) and red signal in panel II refers to MitoTracker Red (excitation at 561); panel III: merged image of panel I and II (pink for overlapped regions) with zoom on a region of interest (indicated by white box). Scale bar: 5 µm.

Declaration of interests

☒ The authors declare that they have no known competing financial interests or personal relationships that could have appeared to influence the work reported in this paper.

☐The authors declare the following financial interests/personal relationships which may be considered as potential competing interests: